ELEMENTA
Science of the Anthropocene

Amiraux, R, et al. 2020. Stress factors resulting from the Arctic vernal sea-ice melt: Impact on the viability of bacterial communities associated with sympagic algae. *Elem Sci Anth*, 8: XX. DOI: https://doi.org/10.1525/elementa.076

RESEARCH ARTICLE

Stress factors resulting from the Arctic vernal sea-ice melt: Impact on the viability of bacterial communities associated with sympagic algae

Rémi Amiraux[1,2,3], Christopher Burot[1], Patricia Bonin[1], Guillaume Massé[3], Sophie Guasco[1], Marcel Babin[3], Frédéric Vaultier[1], and Jean-François Rontani[1,*]

During sea-ice melt in the Arctic, primary production by sympagic (sea-ice) algae can be exported efficiently to the seabed if sinking rates are rapid and activities of associated heterotrophic bacteria are limited. Salinity stress due to melting ice has been suggested to account for such low bacterial activity. We further tested this hypothesis by analyzing samples of sea ice and sinking particles collected from May 18 to June 29, 2016, in western Baffin Bay as part of the Green Edge project. We applied a method not previously used in polar regions—quantitative PCR coupled to the propidium monoazide DNA-binding method—to evaluate the viability of bacteria associated with sympagic and sinking algae. We also measured *cis-trans* isomerase activity, known to indicate rapid bacterial response to salinity stress in culture studies, as well as free fatty acids known to be produced by algae as bactericidal compounds. The viability of sympagic-associated bacteria was strong in May (only approximately 10% mortality of total bacteria) and weaker in June (average mortality of 43%; maximum of 75%), with instances of elevated mortality in sinking particle samples across the time series (up to 72%). Short-term stress reflected by *cis-trans* isomerase activity was observed only in samples of sinking particles collected early in the time series. Following snow melt, however, and saturating levels of photosynthetically active radiation in June, we observed enhanced ice-algal production of bactericidal compounds (free palmitoleic acid; up to 4.8 mg L^{-1}). We thus suggest that protection of sinking sympagic material from bacterial degradation early in a melt season results from low bacterial activity due to salinity stress, while later in the season, algal production of bactericidal compounds induces bacterial mortality. A succession of bacterial stressors during Arctic ice melt helps to explain the efficient export of sea-ice algal material to the seabed.

Keywords: Bacteria, Sea ice, Sympagic algae, Ice biota, Viability, Stress factors, Salinity, Bactericidal free fatty acids, Carbon export

1. Introduction

Primary production in the Arctic Ocean is characterized by short-lived, springtime blooms of sympagic (ice-associated) algae and phytoplankton, which are the major sources of autochthonous organic carbon for the Arctic food web (Horner and Schrader, 1982; Gosselin et al., 1997; Pabi et al., 2008; Wassmann et al., 2011). For both types of microalgae, light availability is the principal factor controlling bloom onset (e.g., Cota, 1985; Lavoie et al., 2005; Lee and Whitledge, 2005; Popova et al., 2010; Campbell et al., 2016), while nutrient availability is the key factor determining its magnitude, duration, and taxonomic composition. The contribution of sympagic algae to total primary production varies depending on the season and the region (from <1% to 60%; e.g., Loose et al., 2011; Dupont, 2012; Fernández-Méndez et al., 2015), but these ice algae represent a crucial food source for the marine food web (Søreide et al., 2010). In sea ice, microalgae are largely concentrated near the ice–water interface within the skeletal layer of the congelation ice, where light is sufficient, the water is relatively rich in nutrients at the start of the bloom season, and physico-chemical conditions (e.g., pH, salinity, temperature) are relatively stable. During the melting season, the high concentrations of extracellular polymeric substances (EPS) they have produced while inhabiting the ice (Ewert and Deming,

[1] Aix-Marseille University, Université de Toulon, CNRS/INSU/IRD, Mediterranean Institute of Oceanography (MIO), Marseille, France

[2] UMR 6539 Laboratoire des Sciences de l'Environnement Marin (CNRS, UBO, IRD, Ifremer) Institut Universitaire Européen de la Mer (IUEM) Plouzané, France

[3] Takuvik Joint International Laboratory, Laval University (Canada)—CNRS, Département de Biologie, Université Laval, Québec, Canada

* Corresponding author:
Email: jean-francois.rontani@mio.osupytheas.fr

2013) favor their agglomeration (Riebesell et al., 1991) and therefore their descent to the seafloor and contribution to sediments. Other scenarios are possible, however, as EPS may also enhance the buoyancy of particles (Riedel et al., 2006; Assmy et al., 2013; Belt et al., 2018).

The fate of algal material in the water column during its sinking depends not only on zooplankton grazing but also on the hydrolytic and remineralization activity of bacteria associated with the sinking particles (whether by sea-ice or water-column bacteria). Howard-Jones et al. (2002) suggested that significant fractions (25%–80%) of Arctic bacterioplankton (including the particle-associated ones) are dormant or express very low activity, based on measurements made in the water column of the Barents Sea marginal ice zone, where the percentage of active bacteria varied by measurement method. Early studies suggested that heterotrophic bacterial remineralization was generally low in perennially cold environments like the Arctic (Pomeroy and Deibel, 1986), allowing organic matter to be exported from productive to oligotrophic regions or to be preserved long enough for use during times of low primary productivity. Subsequent studies have pointed to more complex interactions between temperature and heterotrophic bacterial production and other aspects of bacterial metabolism (Rivkin et al., 1996; Yager and Deming, 1999; Pomeroy and Wiebe, 2001). The effect of temperature on Arctic bacterial activity remains unclear (Kirchman et al., 2005).

In sea ice, some substances produced by ice algae have the potential to inhibit bacterial growth; for example, acrylic acid, which can form during intensive blooms as dimethylsulfoniopropionate (DMSP) is degraded (Monfort et al., 2000), and free fatty acids (FFAs), as produced by some diatoms (Desbois and Smith, 2010). Viral infection may also play a role in the mortality of bacteria in sea ice and the underlying water column (e.g., Maranger et al., 1994; Deming and Collins, 2017). Virus-to-bacteria ratios measured in the bottommost layer of Arctic sea ice are among the highest reported in natural samples (Maranger et al., 1994; Collins and Deming, 2011).

Recently, we suggested that at least for sea-ice bacteria, their limited activity in the Arctic could also result from other stress factors such as salinity (Amiraux et al., 2017). During the early stage of ice melting in spring, brine inclusions become interconnected in channels and experience expulsion from the sea ice into the underlying seawater (Wadhams and Martin, 2001; Ewert and Deming, 2013), which occurs over relatively short timescales (e.g., hours). To cope with the stress of salinity shifts that may be experienced in this ecosystem as a result of brine drainage, bacteria appear to have developed various strategies. Previous work on the microstructure of sea ice raised the possibility that EPS, observed to fill sea-ice pores and coat individual cells inhabiting the brine phase, may provide a physical buffer against extreme salinities (Krembs et al., 2011). Bacteria in sea-ice brines are also able to import or export compatible solutes such as proline, glycine betaine, or choline that can act as osmoprotectants (Ewert and Deming, 2014; Firth et al., 2016). Another major adaptive response of many microorganisms, including bacteria, is to maintain membrane fluidity through "homeoviscous adaptation" (Sinensky, 1974). The shifts in fatty acid composition of membrane lipids, most notably by the enzymatic conversion of *cis*- to *trans*-unsaturated fatty acids (Loffeld and Keweloh, 1996; Heipieper et al., 2003) through the activity of *cis–trans* isomerases (CTI), can constitute an important bacterial mechanism to modify membrane fluidity. To our knowledge, this mechanism has not been studied in the sea-ice environment; however, in other environments, membrane *trans/cis* ratios >0.1 have been suggested to indicate bacterial stress (Guckert et al., 1986).

Within the framework of the Green Edge project, originally designed to investigate the dynamics of the spring bloom in ice-impacted Baffin Bay (Massicotte et al., 2020), we found relatively strong CTI activity (high *trans/cis* ratios) in sea ice and sinking particles collected in the water column during the 2015 vernal melting period, which suggested the occurrence of salinity stress during the early stages of ice melt (Amiraux et al., 2017). The relative stability of these high ratios with depth also suggested that (1) sinking particles were not strongly colonized by pelagic bacteria (unstressed, with low *trans/cis* ratios) and (2) bacterial communities associated with sinking sympagic algae were not growing (as growth is associated with changing *trans/cis* ratios). These two hypotheses are linked, because in the absence of other forms of stress, the *trans/cis* ratio of bacteria decreases to a basic level (Fischer et al., 2010), a decrease that requires de novo synthesis of *cis* fatty acids (Eberlein et al., 2018) and thus bacterial growth. The implication of marine *trans/cis* ratios associated with sinking material remaining at high levels is that growth is not occurring. Nongrowing bacteria, however, are not necessarily inactive metabolically (Kjelleberg et al., 1987), and other forms of stress besides salinity may be involved.

In the 2015 field study (Amiraux et al., 2017), a specific oxidation of the fatty acid palmitoleic acid at position 10 (resulting in the production of 10*S*-hydroxyhexadec-8(*trans*)-enoic acid) was also observed in sea ice and sinking material. This oxidation was attributed to the involvement of a bacterial 10*S*-DOX-like lipoxygenase, initially isolated from *Pseudomonas* 42A2 (Guerrero et al., 1997; Busquets et al., 2004); more recently, the activity of this lipoxygenase has also been observed in members of the genera *Pseudoalteromonas*, *Shewanella,* and *Aeromonas* (Shoja Chaghervand, 2019). The lipoxygenase enzyme, active mainly on free unsaturated fatty acids (Martínez et al., 2010), could play a role in bacterial survival and colonization of environments rich in free fatty acids, such as sympagic algae (Amiraux et al., submitted).

Owing to their high sinking rates and the inferred nongrowing state of their associated bacterial communities, sympagic algae should be relatively preserved during their descent to the seabed and thus contribute perhaps strongly to the benthos and to carbon sequestration at depth. However, the estimation of the bacterial physiological state in the studies cited above was based only on indirect evidence. Here, we evaluated the potential occurrence of the bacterial stressors of salinity and bactericidal

FFAs and their impacts on bacterial viability in sea ice and sinking particles during the 2016 vernal melting season of the Green Edge project. To assess comparative bacterial viability between samples, we used a method not previously applied to these environments—the PMA method, which uses propidium monoazide (PMA), a photoreactive dye that binds to DNA, coupled with quantitative PCR (qPCR) to estimate the percentage of viable and dead bacteria.

2. Materials and methods

2.1. Study site and sampling

Sampling was conducted every 48 h from May 18 to July 8, 2016, at a landfast ice station located near Broughton Island (67° 28.766′N, 63° 47.579′W; water depth of 350 m; **Figure 1**) in Davis Strait within the framework of the Green Edge project. Due to long processing times, samples for the targeted parameters of this study (e.g., bacterial viability and specific lipid content) were taken from sea ice and the water column (sinking particles) on 8 of the 23 sampling dates, from May 18 to June 29. However, these parameters are contextualized by core parameters (e.g., ice and snow thickness, brine salinity and volume, photosynthetically active radiation, chlorophyll *a* concentration, bacterial abundance, common fatty acid content) that were collected on each sampling day. Many of these core parameters have been published elsewhere (Amiraux et al., 2019; Oziel et al., 2019; Massicotte et al., 2020) and are cited specifically in later sections.

2.1.1. Sea ice

On each sampling date, two sets of sea-ice samples for biota were collected using a Kovacs Mark V 14-cm diameter corer and focusing on the bottommost 10 cm of sea ice where the bulk of ice biota are typically found (Smith et al., 1990). The first set of samples were subsectioned into two intervals, 0–3 and 3–10 cm, while the second set focused on the bottommost 0–1 cm of the ice. To compensate for biomass heterogeneity, common in sea ice (Gosselin et al., 1986), 3 or 4 equivalent core sections were pooled for each sampling set on each sampling day and held in isothermal containers until processing. Analyses for chlorophyll *a* (Chl *a*), lipids, and bacterial viability were carried out on the bottom 3-cm sections of the 0–3 and 3–10 cm sampling sets (as well as on the 3–10 cm section for some lipids), while the photosynthetic parameters of sympagic algae were investigated in the 0–1 cm set. At the shore-site laboratory, the pooled sets of the thicker (3 cm) sea-ice sections were melted in dark isothermal containers in filtered seawater (FSW, using 0.2-µm Whatman nucleopore hydrophilic membrane; 3 parts FSW to 1 part ice, vol:vol) to minimize osmotic stress to the microbial community during melting (<12 h; Bates and Cota, 1986; Garrison and Buck, 1987). The pooled sets of the thinner sea-ice sections were melted in dark isothermal containers with a larger relative volume of FSW (ca. 38 parts FSW to 1 part ice, vol: vol) in order to reduce the melting time, which can impact algal physiological photoresponses.

Two additional full ice cores were sampled as described in Miller et al. (2015) to measure vertical profiles of temperature and bulk salinity (Oziel et al., 2019). Ice

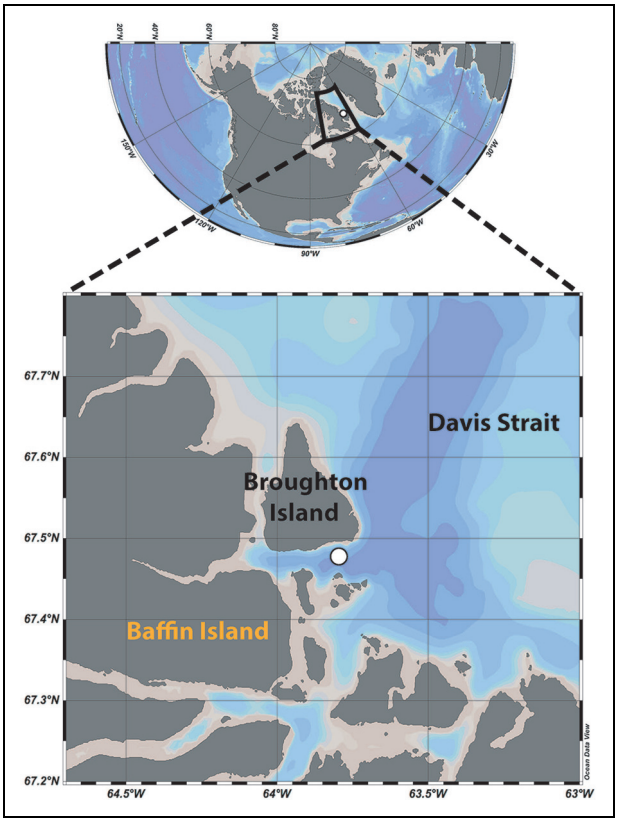

Figure 1. Map of the study area with location of the station investigated in Davis Strait. The white circle on the enlarged map of western Davis Strait indicates the sampling location. DOI: https://doi.org/10.1525/elementa.076.f1

temperature was measured at 10-cm intervals using a high-precision thermometer (Testo 720; ± 0.1 °C). For ice salinity, the ice core was cut with a handsaw into 10-cm sections, which were stored in plastic containers (Whirl-Pak bags) and later melted at room temperature. Bulk (practical) salinity of the melted ice sections was determined using a conductivity probe (Thermo Scientific Orion portable salinometer model WP-84TPS) that was calibrated every sampling day with seawater standard (35) and MilliQ water (0). Brine salinity and volume fraction (%) were calculated for each 10-cm section using the ice temperature and bulk salinity following Cox and Weeks (1983). Salinity of the seawater at the interface with sea ice was obtained using a Sea-Bird Electronics 19plus V2 CTD system (factory calibrated prior to the expedition). The data were post-processed according to the standard procedures recommended by the manufacturer.

Photosynthetically active radiation (PAR) below the sea ice was estimated at 1.3 m using the multispectral data collected with a compact-optical profiling system (C-OPS; version IcePRO; Biospherical instruments, Inc.; see Oziel et al., 2019). To reduce the effects of sea-ice surface heterogeneity on irradiance measurements (e.g., Katlein et al., 2015), the vertical attenuation coefficients of PAR were calculated by fitting a single exponential function on PAR profiles between 10 and 50 m, then used to estimate PAR at 1.3 m (for more details; see Massicotte et al., 2018).

Note that 1.3 m corresponds to the average ice thickness measured during the field campaign and thus to the first measure under the ice (mean = 129 cm; standard deviation [*SD*] = 11 cm, $n = 23$).

2.1.2. Sinking particles

Short-term sediment traps were deployed unfilled and without preservative on a mooring line to collect sinking particles at 2 m and 25 m from below sea ice. Sediment traps were immersed for approximately 48 h and recovered at the same frequency as for the sea-ice sampling sets. Sediment traps were made in-house of polyvinyl chloride (PVC) and had an aperture diameter of 15 cm for a height-to-diameter ratio of 6:7 with a collection cup at the base. Approximately 300 ml was removed from the collection cup on each trap recovery day and subsampled for the different parameters analyzed.

2.2. Chlorophyll a

At the shore-site laboratory, and within 24 h of sampling, duplicate samples of sea ice and sediment trap samples were filtered through Whatman GF/F glass fiber filters. The concentration of Chl *a* retained on the filters was measured using a TD-700 Turner Design fluorimeter, after 18–24 h extraction in 90% acetone at 4 °C in the dark (Parsons et al., 1984). The fluorometer was calibrated with a commercially available Chl *a* standard (*Anacystis nidulans*, Sigma).

2.3. Photosynthetic parameters

To determine photosynthetic parameters, pooled melted 0–1 cm sea-ice samples were incubated at different irradiance levels in the presence of ^{14}C-labeled sodium bicarbonate using a method derived from Babin et al. (1994). Inorganic ^{14}C ($NaH^{14}CO_3$) was added to the samples to achieve a final concentration of approximately 0.7 µCi mL^{-1}. Total initial activity was determined by adding 20-µL aliquots (in triplicate) of the ^{14}C-amended sample to 50 µL of an organic base (ethanolamine), 1 ml of distilled water and 10 ml of scintillation cocktail (EcoLume, MPBiomedicals, San Diego, USA) in glass scintillation vials. Aliquots of the the ^{14}C-amended sample were dispensed into 50-ml cell culture flasks and exposed to a gradient of irradiance provided by LED bulbs (Phillips 9W 6500K dimmable). The incubation system was cooled by circulation of in situ seawater. Scalar PAR irradiance was measured at each position in the incubation chamber prior to the incubation using an irradiance quantum meter (Biospherical QSL-2100, USA) equipped with a 4π spherical collector. After incubating for 120 min, the samples were filtered through 0.2-µm pore-size isopore membrane filters (Milipore, Burlington, USA). Filters were placed in plastic scintillation vials and acidified for 4 h with 500 µl of HCl (6N) to remove excess inorganic carbon. Finally, 10 ml of scintillation cocktail were added to each vial prior to counting in a liquid scintillation counter (Tri-Carb, PerkinElmer, Boston, USA). The carbon fixation rate was then estimated according to Parsons et al. (1984). Photosynthetic parameters, including the saturation parameter (E_k), were estimated from P versus E curves by fitting nonlinear models based on the original definition of Platt and Gallegos (1980).

2.4. Bacterial abundance and viability

Bacterial abundance in the bottom 0–3 cm sea-ice sections was measured by flow cytometry. Samples of the melted ice sections (1.5 ml) were preserved at the shore-site laboratory with a mix of glutaraldehyde and Pluronic F-68 (Gibco; Marie et al., 2014) and stored at –80 °C. Samples were analyzed on a FACS Canto flow cytometer (Becton Dickinson) in the laboratory at the Station Biologique de Roscoff. Bacterial abundance was determined based on the fluorescence of SYBR green-stained DNA (Marie et al., 1997) and corrected for the melt dilution. Measurements of bacterial abundance in the sediment trap samples were not possible to obtain.

For both sea ice and sinking particles, samples for bacterial viability were collected in quadruplicate and treated at the shore-site laboratory. To estimate bacteria viability, we employed the PMA method, adapted from Nocker et al. (2009). The principle is based on the assumption that PMA (phenanthridium, 3-amino-8-azido-5-[3-(diethylmethylammonio)-propyl]-6-phenyl dichloride; Biotium, Inc., Hayward, California, dissolved in 20% dimethyl sulfoxide), when added to a mixture of living and dead (membrane-compromised) cells, selectively enters only the dead cells. Once inside the cells, PMA binds with DNA and can be covalently crosslinked to it by light exposure. PCR amplification of such modified DNA is strongly inhibited. Thus, the comparison of quantitative PCR (qPCR) results obtained for subsamples treated and not treated with PMA provides an estimate of the viability of cells in the sample, quantified as the ratio of living to dead bacteria.

2.4.1. PMA crosslinking

At the shore-site laboratory, sea-ice and sinking particle samples (ca. 10–40 ml), in quadruplicate, were concentrated for the purpose of PMA crosslinking. Samples were pelleted at 5,000 × *g* for 5 min, and the pellets homogenized in 1 ml of 0.2-µm FSW (that had also been autoclaved 1 h at 120 °C after filtration). Two (of four) samples were designated for no treatment and stored at –80 °C, while the other two samples were treated by adding PMA at a final concentration of 100 µM. Following an incubation period of 5 min in the dark at 4 °C with occasional mixing., these samples (1 ml) were filtered through 0.8-µm Whatman nucleopore polycarbonate filters (24 mm, autoclaved 1 h at 110 °C prior to use) to retain attached bacteria on the filters (Bidle and Azam, 1999; Ghiglione et al., 2007). Filters were placed in a Petri dish ™ (Millipore ®) and exposed to light for 2 min using a 650W halogen light source (FAD 120V, 3200K; Osram, light spectrum: 350–800 nm). The samples were placed about 20 cm from the light source and laid horizontally on ice (to avoid excessive heating).

2.4.2. DNA isolation

DNA was extracted from the filter previously obtained (treated or not treated with PMA from sample volumes of 10–40 ml) using DNeasy Blood and Tissue Mini Kits

(Qiagen) according to the manufacturer's instructions. The resulting DNA was kept frozen at –20 °C until further use to enumerate bacteria by quantitative PCR, as described in the next section.

2.4.3 Quantitative PCR

Quantification of the bacterial SSU ribosomal RNA (rRNA) gene was carried out by qPCR with SsoAdvanced™ Sybr Green Supermix on a CFX96 real-time system (C1000 Thermal Cycler, Bio-Rad Laboratories, CA, USA) according to the procedure described in Fernandes et al. (2016). The primers used were DGGE300F (GCCTACGGGAGGCAGCAG; Michotey et al., 2012) and Univ516R sets (GTDTTAC CGCGGCKGCTGRCA; Takai and Horikoshi, 2000). Before amplification, an initial denaturation step of 2 min at 98 °C was performed to activate the polymerase. The real-time PCR cycles consisted of a denaturation step of 5s at 98 °C, a hybridization step of 10s at 55 °C, and an elongation step of 12s at 72 °C for 30 cycles. PCR amplification efficiency was between 96% and 99%. For standard curve construction, a gammaproteobacterial fragment was cloned after purification into pGEMT vector (Promega, WI, USA). After purification, using the Wizard® Plus SV Minipreps Start-Up Kit (Promega), the concentration of plasmids was determined using a NanoDrop™ 1000 spectrophotometer (Thermo Fisher Scientific, DE, USA). The target abundance for standards was calculated using the following formula: gene abundance $= 6.023 \times 10^{23}$ (copies mol^{-1}) $\times$ standard concentration (g mL^{-1}) / molecular mass (g mol^{-1}), assuming that double-stranded DNA has a molecular mass of 660 Da. Standards for bacterial ribosomal gene corresponded to pGEMT plasmids (Promega), harboring one copy of gammaproteobacterial SSU rRNA gene fragment. Data were analyzed by comparative starting quantity of the targeted genes (Table S1). The regression equation was calculated on the graph, plotted between the CT value and the copy number of the standard ranging from 5.78×10^6 to 5.78×10^2 copies in the reaction (Figure S1). At the end of the PCR reactions, the specificity of the amplification was checked from the first derivative of their melting curves and also analyzed by agarose gel electrophoresis.

2.5. Lipid analysis

Due to the number of replicates required to determine bacterial viability (Section 2.4), samples for lipid analysis could not be collected in duplicate. Lipid samples were obtained by filtration through pre-weighed Whatman glass fiber filters (nominal porosity 0.7 μm, 47 mm, combusted for 4 h at 450 °C), with the filters kept frozen (<–20 °C). Owing to the porosity of the filters, these analyses concerned mainly algae (and likely EPS; Meiners et al., 2008) and their attached bacteria (Bidle and Azam, 1999; Ghiglione et al., 2007).

2.5.1. Lipid extraction

Filtered samples were reduced in MeOH (25 ml, 30 min) with excess $NaBH_4$, to reduce labile hydroperoxides (resulting from 10*S*-DOX oxidation) to alcohols, more amenable to analysis using gas chromatography-mass spectrometry (GC-MS). Water (25 ml) and KOH (2.8 g) were then added, and the resulting mixture saponified by refluxing (2 h). After cooling, the mixture was acidified (HCl, 2N) to pH 1 and extracted with dichloromethane (DCM; 3 $\times$ 20 ml). The combined DCM extracts were dried over anhydrous Na_2SO_4 and filtered and concentrated by rotary evaporation at 40 °C to give total lipid extracts (TLEs). Aliquots of TLEs were either silylated and analyzed by gas chromatography-electron impact quadrupole time-of-flight mass spectrometry (GC-QTOF) for lipid quantification, or methylated, then treated with dimethyldisulphide (DMDS) and analyzed by GC-MS/MS for the determination of monounsaturated fatty acid double-bond stereochemistry, as previously described by Amiraux et al. (2017). *Cis* and *trans* isomers of monounsaturated fatty acid methyl esters react with DMDS stereospecifically to form *threo* and *erythro* adducts, which exhibit similar mass spectra but are readily separated by gas chromatography, allowing unambiguous double-bond stereochemistry determination (Buser et al., 1983).

2.5.2. Gas chromatography/tandem mass spectrometry

GC-MS and GC-MS/MS analyses were performed using an Agilent 7890A/7010A tandem quadrupole gas chromatograph system (Agilent Technologies, Parc Technopolis—ZA Courtaboeuf, Les Ulis, France). A cross-linked 5% phenylmethylpolysiloxane (Agilent; HP-5MS ultra inert) (30 m $\times$ 0.25 mm, 0.25-μm film thickness) capillary column was used. Analyses were performed with an injector operating in pulsed splitless mode set at 270 °C. The oven temperature was ramped from 70 °C to 130 °C at 20 °C min^{-1}, then to 250 °C at 5 °C min^{-1} and then to 300 °C at 3 °C min^{-1}. The pressure of the carrier gas (He) was maintained at 0.69×10^5 Pa until the end of the temperature program and then ramped from 0.69×10^5 Pa to 1.49×10^5 Pa at 0.04×10^5 Pa min^{-1}. The following mass spectrometric conditions were used: electron energy 70 eV, source temperature 230 °C, quadrupole 1 temperature 150 °C, quadrupole 2 temperature 150 °C, collision gas (N_2) flow 1.5 ml min^{-1}, quench gas (He) flow 2.25 ml min^{-1}, mass range 50–700 Daltons, cycle time 313 ms. Quantification of DMDS derivatives was carried out in multiple reaction monitoring (MRM) mode. Precursor ions were selected from the more intense ions (and specific fragmentations) observed in electron ionization (EI) mass spectra. *Trans/cis* ratios were obtained directly from peak area measurement (performed several times) of *threo* and *erythro* DMDS adducts.

2.5.3. Gas chromatography–EI quadrupole time of flight mass spectrometry

Accurate mass measurements were carried out in full scan mode using an Agilent 7890B/7200 GC/QTOF System (Agilent Technologies, Parc Technopolis—ZA Courtaboeuf, Les Ulis, France). A cross-linked 5% phenylmethylpolysiloxane (Macherey-Nagel; OPTIMA-5MS Accent; 30 m $\times$ 0.25 mm, 0.25-μm film thickness) capillary column was used. Analyses were performed with an injector operating in pulsed splitless mode set at 270 °C. The oven temperature was ramped from 70 °C to 130 °C

at 20 °C min^{-1} and then to 300 °C at 5 °C min^{-1}. The pressure of the carrier gas (He) was maintained at 0.69 × 10^5 Pa until the end of the temperature program. Instrument temperatures were 300 °C for the transfer line and 230 °C for the ion source. Nitrogen (1.5 ml min^{-1}) was used as collision gas. Accurate mass spectra were recorded across the range *m/z* 50–700 at 4 GHz with the collision gas opened. The QTOF-MS instrument provided a typical resolution ranging from 8,009 to 12,252 from *m/z* 68.9955 to 501.9706. Perfluorotributylamine (PFTBA) was used for daily MS calibration. Quantification of the different lipids (sterols, fatty acids and 10-hydroxyhexadec-8(*trans*)-enoic acid) involved extraction of specific accurate fragment ions, peak integration and determination of individual response factors using external standards ($SD \pm 5\%$).

3. Results

3.1. Sea ice conditions

During the period investigated, snow thickness decreased from 20 cm to 2 cm and ice thickness, from 142 cm to 105 cm (**Figure 2A**). A particularly notable decrease in snow thickness was seen from June 3, ending in its disappearance on June 17. Brine salinity (calculated using the whole sea ice core) decreased throughout the study period from 42.9 to 17.2, while brine salinity in the bottommost 10 cm of sea ice remained relatively constant (mean $\pm$ SD = 29.4 $\pm$ 2.6, n = 21; **Figure 2B**). Depth profiles of brine salinity and of temperature and bulk salinity of the ice are provided in Figure S2. Salinity of the seawater at the interface with sea ice was relatively constant from May 18 to June 10 (mean $\pm$ SD = 32.1 $\pm$ 0.3, n = 12), then decreased from June 13 to July 06 (mean $\pm$ SD = 13.5 $\pm$ 7.0, n = 10; **Figure 2B**), corresponding with the temporal evolution of bulk salinity in the ice (Figure S3). These patterns indicate that release of hypersaline brines from sea ice through brine channels would have occurred prior to June 13, as hypothesized by Amiraux et al. (2019), while the downward percolation of meltwater (hyposaline) took place from ca. June 13 until the end of sampling.

The concentrations of Chl *a* and palmitoleic acid in the bottom 0–3 cm of sea ice were quantifiable throughout the sampling period, with values ranging from 0.9 to 317.3 μg L^{-1} (mean $\pm$ SD = 123.0 $\pm$ 85.2 μg L^{-1}, n = 23) and 0.0 to 36.3 mg L^{-1} (mean $\pm$ SD = 7.1 $\pm$ 8.9 mg L^{-1}, n = 22) (**Figure 2C**), respectively. The lowest sea-ice concentrations of Chl *a* were observed on the last three sampling dates (<4 μg L^{-1}), while the two maxima were observed on June 1 and June 13 (317.3 and 306.9 μg L^{-1}, respectively). The concentration of palmitoleic acid in the bottom 0–3 cm of sea ice, which did not correlate with Chl *a* concentration (r = 0.1, P > 0.5, n = 22), increased from about June 10 and reached a maximum (32.2 mg L^{-1}) on June 20, with a second lesser peak on June 29 (**Figure 2C**). The maximum occurred 3 days after the disappearance of snow (**Figure 2A**), which occurred simultaneously with the first maximum of PAR, as estimated under the ice cover at 1.3 m (**Figure 3**). This under-ice PAR increased from May 18 to June 17 (from 1.6 to 39.3 μE m^{-2} s^{-1}) and again from June 24 to July 08 (from 19.2 to 56.7 μE m^{-2} s^{-1}). Although PAR was relatively low through the beginning of the sampling period, the PAR value required to reach saturating irradiance (E_k) in the 0–1 cm bottommost section of sea ice was measured by June 8 and increased from that date onward to reach *Ek* values of 93.4 and 104.5 μE m^{-2} s^{-1} on June 20 and July 8, respectively.

3.2. Bacterial abundance, stress signals, and viability

Bacterial abundances in the bottommost 3 cm of sea ice increased slowly during May and most of June, with peaks of 7.7 × 10^5 and 9.0 × 10^5 bact mL^{-1} on June 1 and June 13, respectively (**Figure 4**), corresponding to the two maxima observed in Chl *a* concentration (**Figure 2C**). Thereafter, bacterial abundance dropped relatively rapidly to 0.4 × 10^4 bact mL^{-1} by the end of the sampling period (**Figure 4**). Overall, bacterial abundance correlated well with Chl *a* concentration (r = 0.86, P < 0.001).

The *trans/cis* vaccenic acid ratios measured in the bottommost 3 cm of sea ice across the study period fell well below the threshold stress value of 0.1 (mean $\pm$ SD = 0.01 $\pm$ 0.01, n = 8; **Figure 5A**), indicating no stress. In contrast, ratios measured for sinking particles collected at 2 m and 25 m included values from two sampling dates that were clearly above the threshold stress value: 0.29 and 0.36, respectively, on May 18, and 0.15 and 0.15, respectively, on June 1 (**Figure 5B, C**).

The viability of the attached bacterial community inhabiting sea ice appeared to be strong from May 18 to May 27, with only 0%–19% mortality, but weaker in June, with 23%–75% mortality (mean of 43.5 $\pm$ 17.0%, n = 10; **Figure 6A**; Table S1). In the 2-m and 25-m sediment trap samples, bacterial viability was highly variable across the sampling period, with mortality ranges of 0%–64% and 0%–71% at the 2-m and 25-m depths, respectively; **Figure 6B, C**; Table S1).

The fatty acid 10(*S*)-hydroxyhexadec-8(*E*)-enoic acid was quantifiable in most of the samples, whether of sea ice or sinking particles (**Figure 7**). In the sediment trap samples, higher values were observed at the end of the sampling period, on 22 and June 29. The highest concentration 10(*S*)-hydroxyhexadec-8(*trans*)-enoic acid was measured in the deepest (25 m) trap sample on June 22.

3.3. Lipid composition

Fatty acid profiles of the sea-ice samples were dominated by $C_{16:1\Delta9}$ (palmitoleic) and $C_{16:0}$ (palmitic) acids; they also exhibited smaller proportions of $C_{14:0}$, $C_{18:1\Delta9}$, $C_{18:0}$, and $C_{20:5}$ acids (Table S2). Similar fatty acids were also detected in the sediment trap samples, but in different proportions (Table S2). The palmitoleic/palmitic acid ratio was used to estimate the contribution of diatoms to the sinking material (Pedersen et al., 1999; Reuss and Poulsen, 2002). Low values were observed at the beginning of sampling before increasing from June 8 onward, with similar values and temporal patterns observed for the two sampling depths (**Figure 8**). We noted that chromatograms of the lipid fraction of the sinking particles collected at 2 m (Figure S4) and 25 m on June 15 showed the presence of

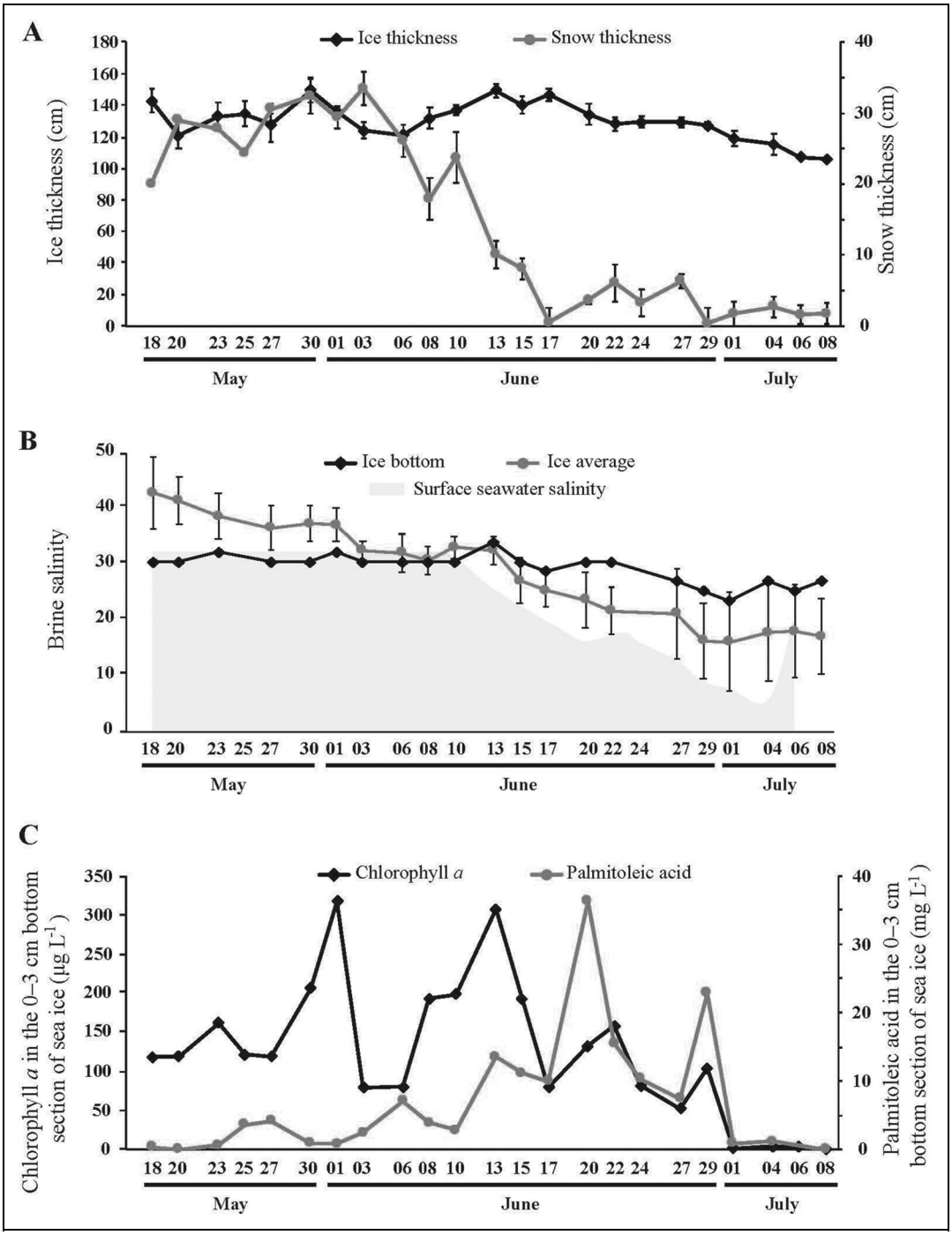

Figure 2. Time series of core parameters and biomarkers in sea ice. Time series of (A) snow ($n = 8–17$) and ice thickness ($n = 8–22$), where error bars are standard deviation (*SD*) of the mean; (B) brine salinity in bottom ice (0–10 cm, black diamonds) and averaged for the whole sea ice core (gray circles), where error bars are *SD* of the mean ($n = 10–15$) and surface seawater salinity is represented in watermark (adapted from Amiraux et al., 2019); and (C) concentrations of Chl *a* and palmitoleic acid in the bottom 0–3 cm sea ice section (3–4 sections pooled prior to analysis) from May 18 to June 08, 2016, at the sampling location in Davis Strait (**Figure 1**). DOI: https://doi.org/10.1525/elementa.076.f2

significant proportions of $C_{20:1}\Delta_{11}$ and $C_{22:1}\Delta_{11}$ alcohols and acids.

The sterol compositions of the different samples were compared to evaluate spatial and temporal changes in algal diversity. We excluded cholesterol from this comparison because of its lack of specificity (Volkman, 1986, 2003) and the possible inputs of this compound during collection and treatment of the samples (Grenacher and Guerin, 1994). Sea-ice samples appeared to be dominated by cholesta-5,24-dien-3β-ol (desmosterol), 24-methylcholesta-5,22(*E*)-dien-3β-ol (brassicasterol), and 24-methylcholesta-5,24(28)-dien-3β-ol (24-methylenecholesterol); they also contained smaller proportions of 24-norcholesta-5,22(*E*)-dien-3β-ol, 24-norcholest-5-en-3β-ol, 24-ethylcholest-5-en-3β-ol (sitosterol), and cholesta-5,22(*E*)-dien-3β-ol (**Figure 9A**). These seven sterols

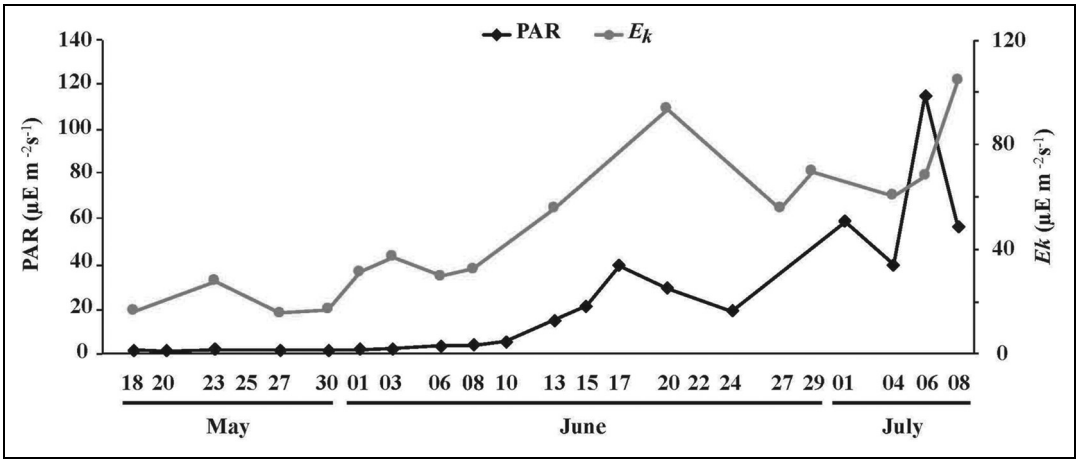

Figure 3. Time series of light parameters in sea ice. Time series of (A) photosynthetically active radiation (PAR, black diamonds) at 1.3 m, underneath the ice (see text); and (B) sympagic algae saturating irradiance (E_k, gray circles) in the bottom (0–1 cm) sea-ice section from May 18 to July 08, 2016, at the sampling location in Davis Strait (**Figure 1**). DOI: https://doi.org/10.1525/elementa.076.f3

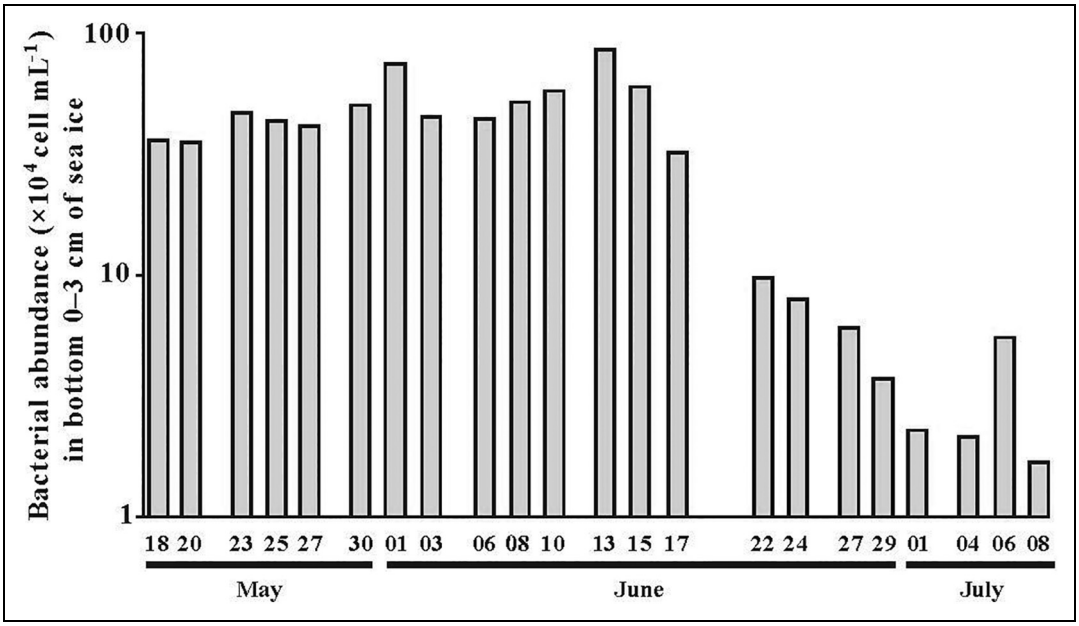

Figure 4. Time series of bacterial abundance in sea ice. Bacterial abundance in the bottom (0–3 cm) sea-ice section from May 18 to June 29, 2016, at the sampling location in Davis Strait (**Figure 1**), where the value for each date represents 3–4 pooled sea-ice sections. Chlorophyll peaks occurred on 1 and June 15, 2016, and concentrations of bactericidal palmitoleic acid increased thereafter (**Figure 2C**). DOI: https://doi.org/10.1525/elementa.076.f4

were also present in sinking particles, but in different proportions (**Figure 9B, C**).

4. Discussion

4.1. Photoacclimation of sympagic algae

During the sampling period, the bottommost 3 cm of sea ice exhibited two periods of particularly high Chl *a* concentration centered on June 1 and 13 (**Figure 2C**; Amiraux et al., 2019). These peaks occurred during a period of relatively stable salinity conditions in the bottommost centimeters of sea ice (Figures 2B and S3). Light and nutrient availability are commonly accepted as the principal factors determining the onset, magnitude, and duration of blooms (Lavoie et al., 2005; Campbell et al., 2016). In light of our results, however, we suggest that the stability of sea-ice salinity may represent another important factor to consider. Although hyposaline conditions are known to significantly impact the sympagic algae (Gosselin et al., 1986; Ralph et al., 2007), the final release of sympagic algae in our study took place in July, well after the release of hyposaline meltwater had begun (**Figure 2B**), and was most likely due to melting sea ice (**Figure 2A**). The occurrence of the second chlorophyll maximum during an advanced snow melting stage

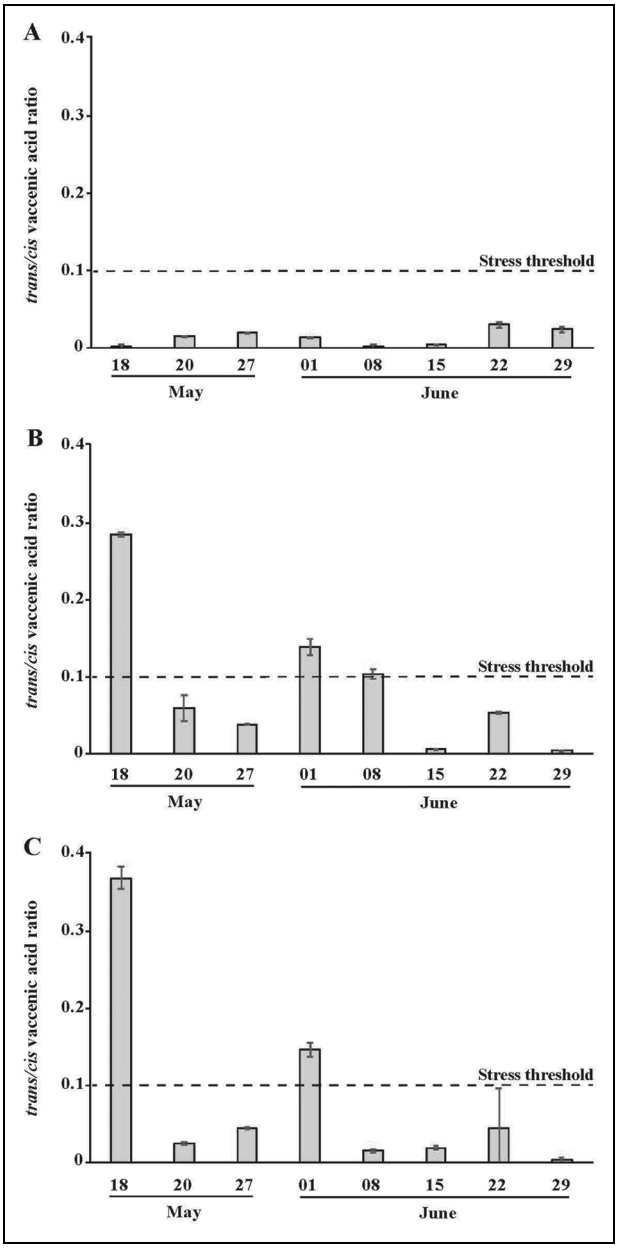

Figure 5. Time series of bacterial osmotic stress signals in sea ice and sinking particles. Time series of *trans/cis* ratios in (A) the bottom (0–3 cm) sea-ice section, and sinking particles collected at (B) 2 m and (C) 25 m from May 18 to June 29, 2016, at the sampling location in Davis Strait (**Figure 1**). The dashed line indicates the threshold stress value of 0.1 as defined by Guckert et al. (1986). Error bars correspond to standard deviation of the dimethyldisulphide (DMDS) derivative peak integration (see text; $n = 3$ for A, B, and C). DOI: https://doi.org/10.1525/elementa.076.f5

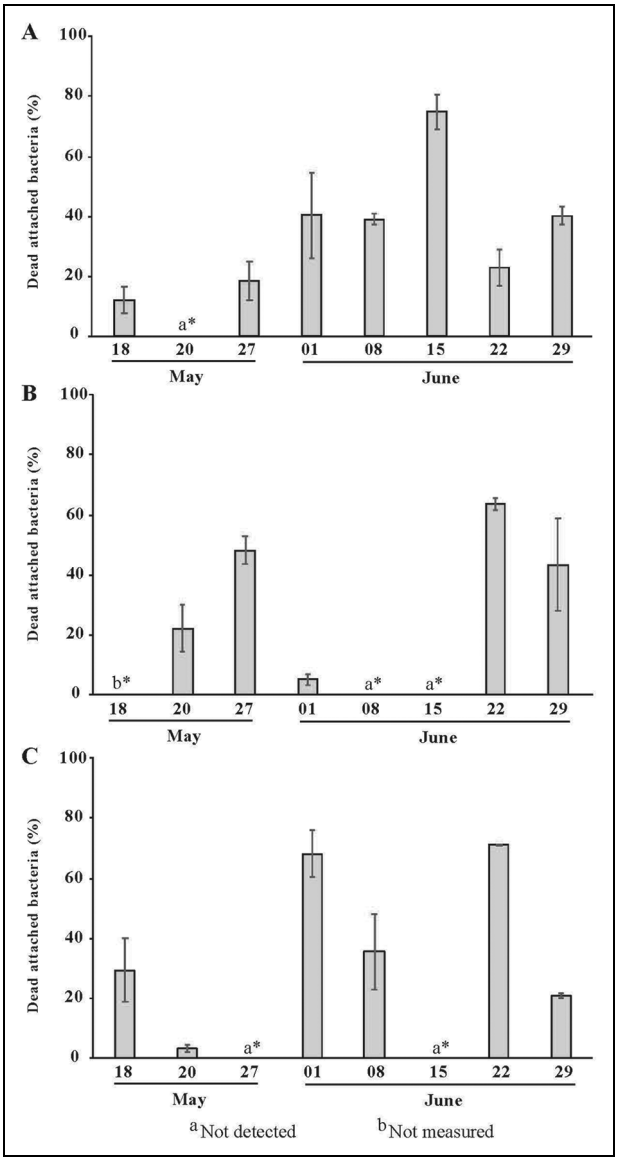

Figure 6. Time series of bacterial viability in sea ice and sinking particles. Time series of the dead percentage of attached bacterial communities in (A) the bottom (0–3 cm) sea-ice section, and in sinking particles collected at (B) 2 m and (C) 25 m from May 18 to June 29, 2016, at the sampling location in Davis Strait (**Figure 1**). Error bars indicate standard deviation ($n = 2$ for A, B, and C); a* indicates not detected; b* indicates not measured. DOI: https://doi.org/10.1525/elementa.076.f6

(**Figure 2A**) is not surprising, as sympagic algae accumulate biomass rapidly when light conditions improve during snowmelt (Mock and Junge, 2007).

Along with Chl *a* concentrations, palmitoleic acid, the major fatty acid of sea-ice diatoms (Fahl and Kattner, 1993; Leu et al., 2010), was also quantified throughout the sampling period. Unlike Chl *a* concentrations, however, palmitoleic acid remained relatively low through May and into June, with order-of-magnitude increases recorded only in the latter part of June, when a lag between the peaks of Chl *a* and palmitoleic acid was evident (**Figure 2C**). Although we cannot reject the possibility that spatial heterogeneity explains these results (the different measurements were made on different cores), the results are consistent with the involvement of photoacclimation processes during this period. Cells acclimated to high light usually exhibit low Chl *a* to C ratios, whereas low-light adapted cells have high ratios because they accumulate pigments to enhance their light absorption efficiency per unit of C biomass (Johnsen and Sakshaug, 1993). Based on

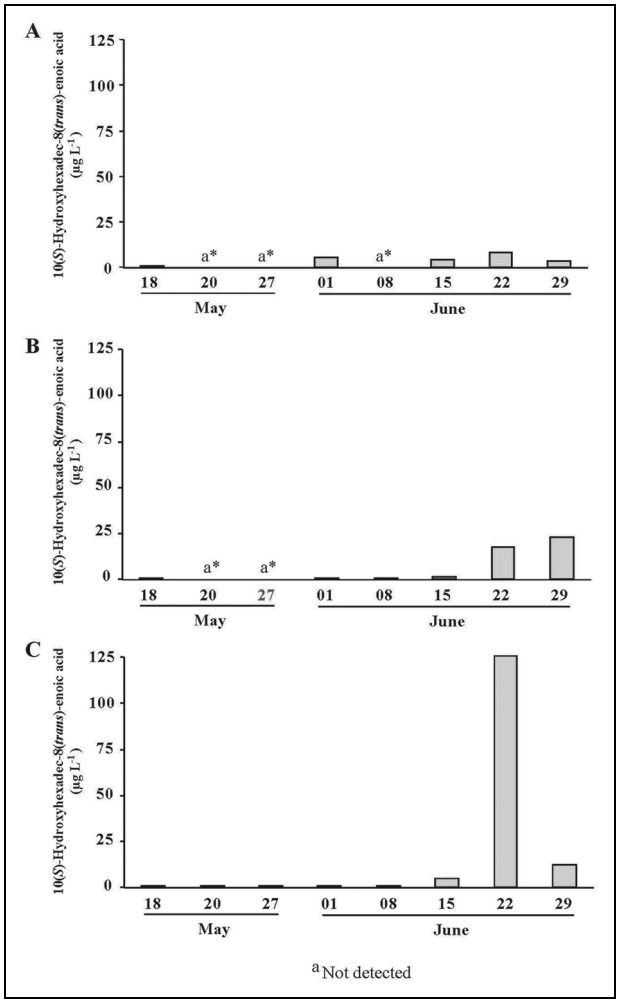

Figure 7. Time series of free fatty acid stress signals in sea ice and sinking particles. Time series of 10(*S*)-Hydroxyhexadec-8(*trans*)-enoic acid concentration in (A) the bottom (0–3 cm) sea-ice section and in sinking particles collected at (B) 2 m and (C) 25 m from May 18 to June 29, 2016, at the sampling location in Davis Strait (**Figure 1**); a* indicates not detected. DOI: https://doi.org/10.1525/elementa.076.f7

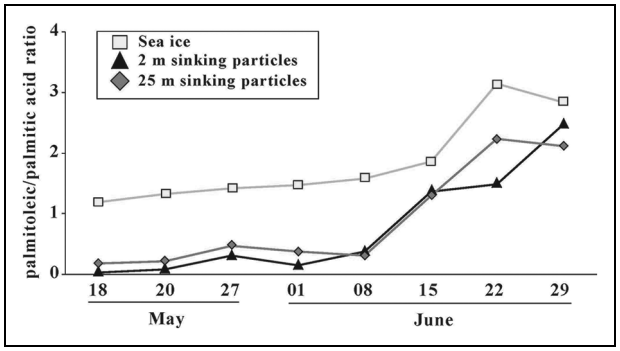

Figure 8. Time series of diatom biomarker in sea ice and sinking particles. Time series of palmitoleic/palmitic acid ratio in (A) the bottom (0–3 cm) sea-ice section and in sinking particles collected at (B) 2 m and (C) 25 m from May 18 to June 29, 2016, at the sampling location in Davis Strait (**Figure 1**). DOI: https://doi.org/10.1525/elementa.076.f8

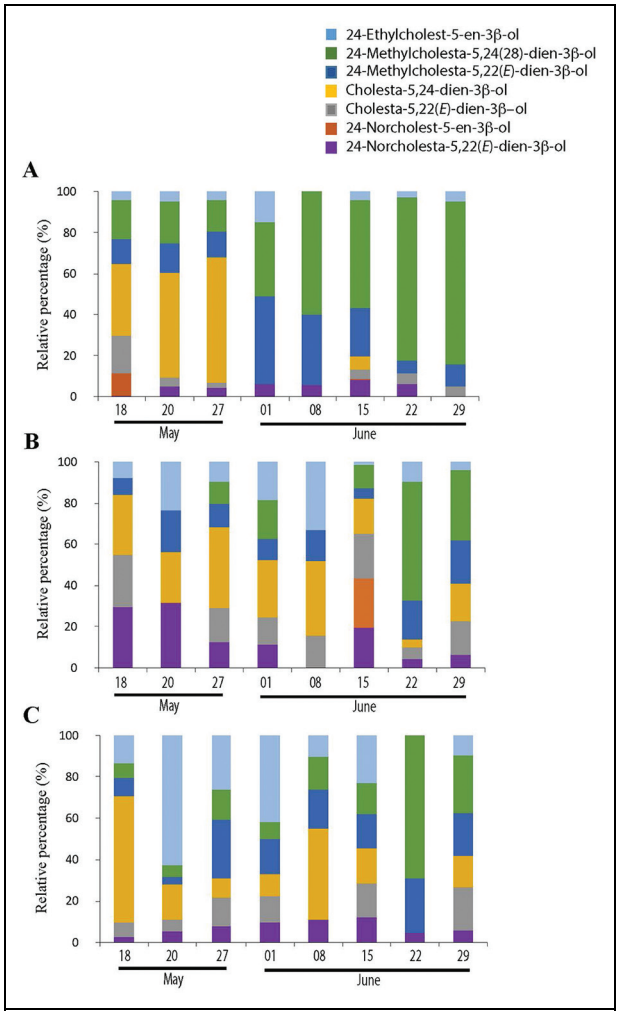

Figure 9. Time series of the Δ^5-sterol composition in sea ice and sinking particles. Time series of the relative Δ^5-sterol composition in (A) the bottom (0–3 cm) sea-ice section and in sinking particles collected at (B) 2 m and (C) 25 m from May 18 to June 29, 2016, at the sampling location in Davis Strait (**Figure 1**). Sterols depicted are sitosterol (24-ethylcholest-5-en-3β-ol (pale blue), 24-methylenecholesterol (24-methylcholesta-5,24(28)-dien-3β-ol, green), brassicasterol (24-methylcholesta-5,22(*E*)-dien-3β-ol, dark blue), desmosterol (cholesta-5,24-dien-3β-ol, yellow), cholesta-5,22(*E*)-dien-3β-ol (gray), 24-norcholest-5-en-3β-ol (orange), and 24-norcholesta-5,22(*E*)-dien-3β-ol (purple).

the rapid disappearance of snow during the first part of June (**Figure 2A**) and the increase in irradiance (PAR) under ice from below 5 to ca. 40 µE m^{-2} s^{-1} by June 17 (**Figure 3**), the sympagic algae represented by the second chlorophyll maximum in mid-June (**Figure 2C**) would be expected to undergo photoacclimation to higher light intensities. The temporal evolution of the sympagic saturating irradiance photosynthetic parameter (E_k) in the bottommost 0–1 cm of sea ice during this period strongly supports this expectation. Because the bottommost 0–1 cm section of sea ice receives less light than upper sections (e.g., light-shading from ice algae; Perovich, 1996), the increase in E_k measured in the 0–1 cm section from

mid-June until the end of sampling (**Figure 3**) suggests that E_k in the 0–3 cm section would have been even higher. The photoacclimation result is also consistent with the photoacclimation of sympagic algae to higher light intensities, and the consequent reduction of their Chl *a* content per cell is consistent with the observed mismatch between Chl *a* and palmitoleic acid peaks (**Figure 2C**).

In algae, increasing light intensities also induce a decrease in their total polar lipid content, with a concomitant increase in the amounts of neutral storage lipids, the triacylglycerols (TAGs), and free fatty acids (FFAs; Brown et al., 1996; Khotimchenko and Yakovleva, 2005; Hu et al., 2008). The high irradiance resulting from the disappearance of snow cover on June 17 should thus induce a concomitant decrease in Chl *a* content per cell due to photoacclimation and an accumulation of TAGs and FFAs, including palmitoleic acid, as observed in **Figure 2C**.

4.2. Stress and resulting viability of the attached bacterial community in sea ice

In this study, we defined the term of attached bacteria on the basis of filtration using a filter pore size of 0.8 µm. This operational definition allows retention of most particle aggregates and their attached bacteria. However, free-living bacteria may also be retained as a consequence of filter clogging, with the fraction of retained free-living bacteria generally assumed to increase with the volume of sample filtered. Here, sample volumes of less than 40 ml were filtered with no evidence of clogging, so we assume that free-living bacteria were a negligible component in the analysis of bacteria called "attached."

Regarding total bacterial abundance in the bottommost 3 cm of sea ice, limited increases were observed during the sampling period associated with the chlorophyll maxima (**Figure 4**), and bacterial production was relatively weak (F Joux, personal communication; GreenEdge meeting, 2019). Although hinting at a degree of stress to the bacterial community, such bulk measurements are less likely to reveal stress responses than more specific measurements targeting a subset of the community, in particular the attached bacteria.

Bacteria inhabiting brine channels in ice are exposed to highly variable salinity, pH, and dissolved inorganic nutrient concentrations (Thomas and Papadimitriou, 2003). One of the adaptive responses of bacteria to changes in salinity is to keep their membrane fluidity at a constant value through "homeoviscous adaptation" (Heipieper et al., 2003), a process facilitated by conversion of *cis* to *trans* unsaturated fatty acids (Loffeld and Keweloh, 1996). Indeed, a *trans/cis* fatty acid ratio >0.1 was proposed previously as an indicator of bacterial stress (Guckert et al., 1986). The very low values of the *trans/cis* ratio of vaccenic acid, a fatty acid specific to bacteria (Sicre et al., 1988), observed in our sea-ice samples (**Figure 5A**) suggest that bacteria attached to sympagic algae in the bottommost sections of the ice were not experiencing osmotic stress during the sampling period. This interpretation is consistent with the stable brine salinities of that layer of sea ice throughout the sampling period (**Figure 2B**). Even higher in the ice, brine salinities were not extreme (maximum of ca. 43, on the first day of sampling; **Figure 2B**). Consequently, the high mortality measured during June (mean of 44%), using the PMA method coupled with qPCR (**Figure 6A**), must be attributable to a different stress.

A role for viruses in the mortality of sympagic bacteria cannot be excluded and may have been likely (Maranger et al., 1994); however, the mortality we observed was based on the percentage of intact cells that were nonfunctional (dead) due to compromised membranes. Bacteria lysed (no longer intact) by viruses would not have been included in these percentages. Bacterial mortality associated with sympagic algae could also result from the algal release of toxic compounds such as acrylic acid (degradation product of DMSP; Monfort et al., 2000) or FFAs (Desbois and Smith, 2010). However, concentrations of DMSP and dimethyl sulfide (DMS; degradation product of DMSP; Lizotte et al., 2017) in sea ice are generally well correlated with Chl *a* concentrations (Tison et al., 2010). An induction of acrylic acid-induced stress when Chl *a* concentration was low (**Figure 2C**) thus seems unlikely, nor did the presence of *Phaeocystis*, a known producer of copious amounts of DMSP, dimethylsulfide and acrylic acid, appear sufficient to influence the bacterial community (reaching only 1.5% and 3.6% of the protist community on June 20 and 29, respectively; M Babin, personal communication; GreenEdge meeting, 2019).

Instead, the presence of FFAs, produced by sympagic algae as a significant proportion of their lipid content (Falk-Petersen et al., 1998) which can be amplified during late bloom conditions (Smith et al., 1993) or under high irradiation (Hu et al., 2008), could be at the origin of this stress. FFAs are released from cellular lipids by host lipolytic enzymes (Jüttner, 2001; Wichard et al., 2007). They are toxic for many bacteria owing to their deleterious effect on bacterial cellular membranes (Greenway and Dyke, 1979; Chamberlain et al., 1991). They can also inhibit enzyme activity, disrupt electron transport chains, and uncouple oxidative phosphorylation (reviewed by Desbois and Smith, 2010). In general, unsaturated FFAs tend to have greater antibacterial potency than saturated FFAs with the same carbon chain length (Desbois et al., 2009), and the most potent usually have 14 or 16 carbon atoms (Feldlaufer et al., 1993). Free palmitoleic acid, a monounsaturated 16-C FFA, displays strong bactericidal action against Gram-negative marine bacterial pathogens, as reported by Desbois et al. (2009). Sympagic algal production of this FFA (stimulated by increasing irradiance) could thus contribute to the high mortality (approximately 75%) of attached bacteria observed on June 15 (**Figure 6A**).

To test this hypothesis, we quantified free palmitoleic acid in samples collected on June 1 and 15 during the two chlorophyll peaks. The concentrations measured (0.3 and 4.8 mg L^{-1}, respectively) support elevated bactericidal activity during the second chlorophyll peak. Although the basic nature of seawater has been proposed to enhance the solubility and thus toxicity of FFAs (Parrish, 2013), the effect may be stronger in sea-ice brines where the pH

varies between 8.0 and 8.5 (Hare et al., 2013). The proximity of bacteria to sympagic algae cells (attached bacteria) would also make them particularly susceptible to the antibacterial activity of free palmitoleic acid. Indeed, FFAs released by host lipolytic enzymes from a microalgal cell generally act on bacterial pathogens in the local vicinity (Desbois and Smith, 2010).

4.3. Stress and resulting viability of attached bacteria in sinking particles

The algal material present in sinking particles collected by the sediment traps was less than the material present in bottom sea ice, based on Chl *a* concentrations (<1.2 μg L^{-1} until June 24 near the end of the time series, as reported by Amiraux et al., 2019). The presence of diatoms, the dominant taxa of sympagic and planktonic blooms in the Arctic (Sakshaug, 2004; Mikkelsen et al., 2008; Tremblay et al., 2012), could be estimated using the palmitoleic/palmitic acid ratio, however, as employed by others to follow diatom blooms (Pedersen et al., 1999; Reuss and Poulsen, 2002). Our results showed an increase in diatoms in sinking particles from early June onward (**Figure 8**). Concentrations of IP_{25}, the specific tracer of sympagic diatoms (Belt and Müller, 2013; Belt, 2018) measured in the same samples (Amiraux et al., 2019), supported sea ice as the source of this sinking material. Amiraux et al. (2019) suggested that the flush of sympagic algae into the water column resulted from shifts in the salinity of sea-ice brines likely induced by the downward percolation of melted snow and, from June 24, to melting of the sea-ice skeletal layer (**Figure 2A, B**). The resulting hyposaline stresses, known to reduce sympagic algal growth and survival (Gosselin et al., 1986), would favor their release from the ice as well as their potential agglomeration (Riebesell et al., 1991).

High *trans/cis* vaccenic acid ratios were previously observed in sinking particles collected a year earlier during the 2015 GreenEdge campaign (Amiraux et al., 2017). These high values were attributed to the release of sympagic algae with attached bacteria stressed by hypersaline brines during the early stages of sea ice melting. In the present study, the investigation of this ratio showed high values only on the first day of the time series (May 18; **Figure 5B, C**) when brine salinity was also highest (**Figure 2B**). The relatively high *trans/cis* ratios measured at the start of the time series in the 3–10 cm section of ice (approximately 0.15, above the threshold indicative of stress; Figure S5) suggests that sinking particles derived from brine channels during the beginning of the melting season. During the latter part of the time series (June 15–29) when most ice-algal material was released and settling, the *trans/cis* ratio remained very low, attesting to the lack of salinity stress (or other stressors). We thus attribute the high mortality of attached bacteria observed in sinking particles from the last two sampling dates in June (**Figure 6B, C**) to the presence of free palmitoleic acid at depth. Unfortunately, the fraction of sediment trap material available for lipid analyses was too low to allow quantification of FFAs, including palmitoleic acid. However, the likely presence of an elevated proportion of FFAs in the sinking material is supported by the increase in 10(*S*)-hydroxyhexadec-8(*trans*)-enoic acid concentration observed on June 22 (**Figure 7**), when most of the sinking material appeared to be composed of sympagic material (based on IP_{25}; Amiraux et al., 2019). Fatty acids are thought to bind to 10*S*-DOX-like lipoxygenase with their carboxyl groups at a fixed position relative to the catalytic site, allowing the enzyme to contribute to the detoxification of fatty acids in the bacterial environment (Martínez et al., 2010). The increase in 10(*S*)-hydroxyhexadec-8(*trans*)-enoic acid concentration observed with depth (**Figure 7**), indicative of 10*S*-DOX-like lipoxygenase activity, is consistent with the proposed elevated proportions of free palmitoleic acid in sinking particles.

Because the highest sinking fluxes of sympagic algae were observed from June 15 onward (Amiraux et al., 2019), we analyzed the samples from this period in greater depth. The mortality of attached bacteria in sinking particles collected on June 22 and 29 was clearly elevated (**Figure 6B, C**), yet no mortality was detected in the sediment trap samples collected on June 15. The high mortality in sea ice observed on this date was not matched by enhanced mortality in sinking particles. This discrepancy could be attributed to (1) a bulk dilution of dead bacteria associated with sympagic algae by living bacterial inputs (i.e., bacteria associated with phytoplankton or copepod fecal pellets) or (2) a lag in sedimentation.

To estimate the relative contribution of sympagic algae, phytoplankton, and zooplankton to these samples, Δ^5-sterol compositions of corresponding sea-ice and sinking particle samples were compared (**Figure 9**). Three sterol profiles were observed in the sea ice during the time series. The first profile between May 18 and 27 was characterized by the dominance of desmosterol (**Figure 9**) and cholesterol (data not shown), suggesting the presence of sympagic amphipods (Harvey et al., 1987) known to live in sea-ice brine channels (Macnaughton et al., 2007). The second, observed from June 1 to 8, was mainly composed of pennate diatoms (dominated by *Nitzschia frigida*; B Queguiner, personal communication; GreenEdge meeting, 2019) as suggested by the dominance of brassicasterol and 24-methylenecholesterol (Rampen et al., 2010). The third community, from June 15 to 29, showed an increasing contribution of centric diatoms (*Melosira arctica*), as suggested by the dominance of 24-methylenecholesterol (Rampen et al., 2010). The similarities of sterol profiles observed in sea-ice and sediment traps collected on June 22 attest to the dominance of sympagic algae in sinking particles, as well as their rapid descent (Amiraux et al., 2019).

In contrast, the sterol compositions of trap samples collected on June 15 and 29 differed from those of the corresponding sea-ice samples by their higher contents of 24-norcholesta-5,22(*E*)-dien-3β-ol, 24-norcholest-5-en-3β-ol, desmosterol and cholesta-5,22(*E*)-dien-3β-ol) (**Figure 9**). These differences suggested the presence of high and moderate proportions of phytoplankton in trap samples collected on June 15 and 29, respectively. On the basis of number of epiphytic bacteria per algal cell, generally one order of magnitude higher for ice diatoms (up

to 25 in Arctic sea ice; Smith et al., 1989) compared to phytoplankton (<2; Kaczmarska et al., 2005), a bulk dilution of bacteria attached to sympagic algae by unstressed bacteria attached to phytoplankton seems unlikely on June 15. This conclusion is supported by the relatively high bacterial mortality observed in sinking particles collected later, on June 29, which were composed, at least in part, of phytoplankton (under-ice bloom from June 24; Amiraux et al., 2019).

Lipid extracts of sinking particles collected on June 15 showed the presence of $C_{20:1}\Delta_{11}$ and $C_{22:1}\Delta_{11}$ alcohols and acids (Figure S4), known to occur in herbivorous copepods that undergo diapause (Graeve et al., 1994), and a high proportion of sterols relative to fatty acids (Figure S4), as often observed after copepod feeding on phytoplankton (Bradshaw et al., 1991). These results suggest that the samples collected on June 15 contained copepod fecal pellets, a favorable environment for bacterial growth; indeed, incubation of copepods collected in the water column near this date exhibited maximum production of fecal pellets (Sampei et al., submitted). Because fecal pellets increase the sedimentation rate of particulate matter (Small et al., 1979), the lack of bacterial mortality in sinking particles collected on June 15 seems unlikely to be due to a lag in sedimentation. We thus attribute the lack of detectable bacterial mortality in sinking particles from this date to bulk dilution of stressed bacteria attached to sympagic algae by fecal pellet-colonizing bacteria.

4.4. Impact of bacterial stress on the preservation of sympagic material

Following the use of *cis-trans* isomerase activity as an urgent response to guarantee survival against stress, bacteria replace this short-term activity with other adaptive mechanisms (Heipieper et al., 2007). Consequently, in the absence of osmotic stress in the water column (after release from exposure to any higher brine salinity in sea ice), the *trans/cis* ratio of salinity-stressed bacteria associated with sympagic algae should decrease to the basic level (as for other bacteria; Fischer et al., 2010). If the conversion of *trans* to *cis* fatty acids is no longer being catalysed (Eberlein et al., 2018), then recovery to the regularly low *trans/cis* ratio requires *de novo* synthesis of *cis* fatty acids, which is dependent on bacterial growth. The stability of the *trans/cis* ratio previously observed associated with sinking particles during the 2015 vernal melting period at our same sampling site was thus attributed to the nongrowing state of attached bacteria (Amiraux et al., 2017). The high *trans/cis* ratios measured in sinking particles collected in this study on May 18, 2016 (0.29 and 0.36 at 2-m and 25-m depth, respectively; **Figure 5B, C**), again points to the nongrowing state of bacteria attached to sinking material during the early stages of ice melt. Most of these attached bacteria remained viable (**Figure 4**), as PMA did not enter the cells to bind to DNA and thus inhibit PCR amplification (Nocker et al., 2006).

In contrast, by the end of the melting season, the PMA technique showed that most of the bacteria associated with sympagic algae had disrupted membranes and were considered dead. Because osmotic stress appeared to be lacking at this time, free palmitoleic acid produced by the ice algae can explain the strongly altered membranes of these bacteria. The insertion of FFAs into the inner bacterial membrane increases its permeability, allowing internal contents to leak from the cell, which can result in growth inhibition or death (Shin et al., 2007).

Overall, our study suggests that the bacterial community associated with sympagic algae is exposed to multiple stresses during most of the vernal Arctic melting season. This exposure reduces their viability, as indicated by the nonreversible loss of membrane integrity, thereby limiting their potential to remineralize sympagic algal material. We hypothesize that the fate of sympagic algae during a complete melting cycle of the ice occurs in successive steps as follows: (1) During the beginning of ice melt, a limited amount of sympagic algae is discharged into the water column, and bacteria attached to the sinking algae are nongrowing due to osmotic stress from prior exposure to hypersaline sea-ice brine. (2) At the end of snow cover melt, sympagic algae bloom, followed by a photoacclimation phase that induces the production of bactericidal FFAs. (3) The downward percolation of melted snow generates hyposaline conditions that cause sympagic algae to aggregate. (4) The aggregated sympagic algae flush into the water column, with their attached bacteria strongly impacted by bactericidal FFAs, which may even increase with depth.

5. Conclusions

During this work, we evaluated the viability of bacteria in sea ice and in sinking particles over the course of a spring ice melt season, from May 18 to June 29, 2016, in Davis Strait, Canadian Arctic. In mid-June, just after the second of two chlorophyll peaks in the ice, an intense production of palmitoleic acid, mainly esterified in TAGs but also present in free form, was detected and attributed to the effects of excess irradiance induced by the complete disappearance of snow cover. The viability of the attached bacterial community in sea ice, quantified by the PMA approach coupled with qPCR, showed high mortality (up to 75%, mean of 44%) toward the end of ice melting. We attribute the mortality of these attached bacteria to the bactericidal properties of free palmitoleic acid released by sympagic algae under the effect of light stress. Osmotic stress to bacteria in sea-ice brines appeared to be limited to the beginning of ice melt, which could be tested in future by applying our suite of measurements to sea ice prior to the melting season. Due to their propensity for strong aggregation (shortening residence time within the water column) and the high mortality of their attached bacteria (limiting remineralization), sympagic algae should contribute importantly to the export of carbon to Arctic sediments.

Data accessibility statement

All data are accessible at the Green Edge database (http://www.obs-vlfr.fr/proof/php/GREENEDGE/greenedge.php) and will be made public prior to publication.

Supplemental files

The supplemental files for this article can be found as follows:

Figure S1. qPCR calibration curves for determining the number of bacterial 16S rDNA genes. Example of (A) relative fluorescence versus cycle number. Amplification curves are created when the fluorescent signal from each sample is plotted against cycle number; therefore, amplification plots represent the accumulation of product over the duration of the real-time PCR experiment. The samples used to create the plots are a dilution series of the target DNA sequence. Example of (B) a standard curve of real-time PCR data. A standard curve shows threshold cycle (Ct) on the *y*-axis and the starting quantity (SQ) of DNA target on the *x*-axis. Slope, *y*-intercept, and correlation coefficient values are used to provide information about the performance of the reaction.

Figure S2. Temporal evolution of sea-ice properties. Time series of (A) sea-ice temperature, (B) bulk salinity, and (C) brine salinity as a function of depth, where mean sea-ice thickness is indicated by the black line (adapted from Oziel et al., 2019).

Figure S3. Temporal evolution of mean bulk salinity in sea ice. Time series of mean bulk salinity in the whole sea-ice core. Error bars are standard deviation of the mean ($n = 11–15$).

Figure S4. TIC chromatogram of the total lipid extract in sinking particles. TIC chromatogram of the total lipid extract of sinking particles collected at 2 m on June 15, showing the presence of $C_{20:1\Delta11}$ and $C_{22:1\Delta11}$ alcohols and acids.

Figure S5. Time series of bacterial osmotic stress signals in the near-bottom 3–10 cm sea-ice section. Time series of *trans/cis* ratios in the near-bottom 3–10 cm sea-ice section from May 18 to June 29, 2016, at the sampling location in Davis Strait (**Figure 1**). The dashed horizontal line indicates the threshold stress value of 0.1 as defined by Guckert et al. (1986). Error bars represent the standard deviation of the dimethyldisulphide (DMDS) derivative peak integration ($n = 3$).

Table S1. qPCR raw data for determination of the percentage of dead bacteria.

Table S2. Relative fatty acid composition of sea ice and sediment trap samples.

Acknowledgments

The GreenEdge project is funded by the following French and Canadian programs and agencies: ANR (contract #111112), CNES (project #131425), IPEV (project #1164), CSA, Fondation Total, ArcticNet, LEFE, and the French Arctic Initiative (GreenEdge project). This project was made possible by the support of the hamlet of Qikiqtarjuaq and the members of the community together with the Inuksuit School and its Principal Jacqueline Arsenault. It was conducted under the scientific coordination of the Canada Excellence Research Chair on Remote Sensing of Canada's new Arctic frontier and the CNRS & Université Laval Takuvik Joint International Laboratory (UMI3376). The field campaign owed its success to the contribution of J. Ferland, G. Bécu, C. Marec, J. Lagunas, F. Bruyant, J. Larivière, E. Rehm, S. Lambert-Girard, C. Aubry, C. Lalande, A. LeBaron, C. Marty, J. Sansoulet, D. Christiansen-Stowe, A. Wells, M. Benoît-Gagné, E. Devred, and M.-H. Forget from the Takuvik Laboratory; C. J. Mundy from the University of Manitoba; and F. Pinczon du Sel and E. Brossier from Vagabond. We also thank Québec-Océan, the CCGS *Amundsen*, and the Polar Continental Shelf Program for their in-kind contribution in polar logistics and scientific equipment. We especially thank C. Nozais from the Université du Québec à Rimouski for providing the sediment traps and C. Lalande (Project leader), C. Aubry, and T. Dezutter from the Université Laval Joint International Laboratory and Takuvik Laboratory for allowing the 2016 short-term sediment trap deployment. We thank D. Vaulot, M. Tragin, and D. Marie for providing cytometry data. Thanks are also due to the FEDER OCEANOMED (No. 1166-39417) for the funding of the GC-QTOF and GC-MS/MS employed. We are grateful to the editors and the two anonymous reviewers for providing helpful comments on a previous version of the manuscript.

Funding information

This work received financial support from the Université Bretagne Loire (UBL) "post-doctoral attractiveness" program and the Sentinel North postdoctoral program of Université Laval, made possible in part by funding from the Canada First Research Excellence Fund. This work was also supported by the Bacstress (INSU—EC2CO-Microbien) and Green Edge projects. The Green Edge project is funded by the following French and Canadian programs and agencies: ANR (Contract #111112), CNES (project #131425), IPEV (project #1164), CSA, Foundation Total, ArcticNet, LEFE, and the French Arctic Initiative (Green Edge project).

Competing interests

The authors declare that they have no competing interests.

Author contributions

Design of the study: RA, J-FR, PB, and MB.
Writing: RA, J-FR, and PB.

RA led the analysis of lipids with contributions from CB, GM, FV, J-FR.

RA led the analysis of bacterial viability with contributions from SG and PB.

All authors revised the earlier version of the manuscript, helped in the interpretation, and approved the final version for publication.

References

Amiraux, R, Belt, ST, Vaultier, F, Galindo, V, Gosselin, M, Bonin, P, Rontani, J-F. 2017. Monitoring photo-oxidative and salinity-induced bacterial stress in the Canadian Arctic using specific lipid tracers. *Mar Chem* **194**: 89–99. DOI: http://dx.doi.org/10.1016/j.marchem.2017.05.006.

Amiraux, R, Rontani, J-F, Armougom, F, Frouin, E, Babin, M, Artigue, L, Bonin, P . Monitoring of biodiversity and stress state of bacteria associated with

ice algae and sinking particles in the Canadian Artic. *Elem Sci Anth* (under review).

Amiraux, R, Smik, L, Köseoğlu, D, Rontani, J-F, Galindo, V, Grondin, P-L, Babin, M, Belt, ST. 2019. Temporal evolution of IP25 and other highly branched isoprenoid lipids in sea ice and the underlying water column during an Arctic melting season. *Elem Sci Anth* **7**(1): 38. DOI: https://doi.org/10.1525/elementa.377.

Assmy, P, Ehn, JK, Fernández-Méndez, M, Hop, H, Katlein, C, Sundfjord, A, Bluhm, K, Daase, M, Engel, A, Fransson, A, Granskog, MA, Hudson, SR, Kristiansen, S, Nicolaus, M, Peeken, I, Renner, AHH, Spreen, G, Tatarek, A, Wiktor, J. 2013. Floating ice-algal aggregates below melting Arctic sea ice. *PLoS One* **8**(10). DOI: https://doi.org/10.1371/journal.pone.0076599.

Babin, M, Morel, A, Gagnon, R. 1994. An incubator designed for extensive and sensitive measurements of phytoplankton photosynthetic parameters. *Limnol Oceanogr* **39**(3): 694–702. DOI: https://doi.org/10.4319/lo.1994.39.3.0694.

Bates, SS, Cota, GF. 1986. Fluorescence induction and photosynthetic responses of Arctic ice algae to sample treatment and salinity. *J Phycol* **22**(4): 421–429. DOI: https://doi.org/10.1111/j.1529-8817.1986.tb02484.x.

Belt, ST, Brown, TA, Smik, L, Assmy, P, Mundy, C. 2018. Sterol identification in floating Arctic sea ice algal aggregates and the Antarctic sea ice diatom *Berkeleya adeliensis*. *Org Geochem* **118**: 1–3. DOI: https://doi.org/10.1016/j.orggeochem.2018.01.008.

Belt, ST, Müller, J. 2013. The Arctic sea ice biomarker IP_{25}: A review of current understanding, recommendations for future research and applications in palaeo sea ice reconstructions. *Quat Sci Rev* **79**: 9–25. DOI: http://dx.doi.org/10.1016/j.quascirev.2012.12.001.

Belt, ST. 2018. Source-specific biomarkers as proxies for Arctic and Antarctic sea ice. *Org Geochem* **125**: 277–298. DOI: https://doi.org/10.1016/j.orggeochem.2018.10.002.

Bidle, KD, Azam, F. 1999. Accelerated dissolution of diatom silica by marine bacterial assemblages. *Nature* **397**(6719): 508–512. DOI: https://doi.org/10.1038/17351.

Bradshaw, SA, Eglinton, G, O'Hara, SC, Corner, ED. 1991. Biogeochemical changes in lipids in a model marine food chain. *Dev Geochem* **6**: 49–58.

Brown, MR, Dunstan, GA, Norwood, SJ, Miller, KA. 1996. Effects of harvest stage and light on the biochemical composition of the diatom *Thalassiosira pseudonana*. *J Phycol* **32**(1): 64–73. DOI: https://doi.org/10.1111/j.0022-3646.1996.00064.x.

Buser, HR, Arn, H, Guerin, P, Rauscher, S. 1983. Determination of double bond position in monounsaturated acetates by mass spectrometry of dimethyl disulfide adducts. *Anal Chem* **55**(6): 818–822.

Busquets, M, Deroncele, V, Vidal-Mas, J, Rodriguez, E, Guerrero, A, Manresa, A. 2004. Isolation and characterization of a lipoxygenase from *Pseudomonas 42A2* responsible for the biotransformation of oleic acid into (*S*)-(*E*)-10-hydroxy-8-octadecenoic acid. *Antonie Van Leeuwenhoek* **85**(2): 129–139. DOI: https://doi.org/10.1023/B: ANTO.0000020152.15440.65.

Campbell, K, Mundy, C, Landy, J, Delaforge, A, Michel, C, Rysgaard, S. 2016. Community dynamics of bottom-ice algae in Dease Strait of the Canadian Arctic. *Prog Oceangr* **149**: 27–39. DOI: https://doi.org/10.1016/j.pocean.2016.10.005.

Chamberlain, NR, Mehrtens, BG, Xiong, Z, Kapral, FA, Boardman, JL, Rearick, JI. 1991. Correlation of carotenoid production, decreased membrane fluidity, and resistance to oleic acid killing in *Staphylococcus aureus* 18Z. *Infect Immun* **59**(12): 4332–4337.

Collins, RE, Deming, JW. 2011. Abundant dissolved genetic material in Arctic sea ice Part II: Viral dynamics during autumn freeze-up. *Polar Biol* **34**(12): 1831–1841. DOI: https://doi.org/10.1007/s00300-011-1008-z.

Cota, GF. 1985. Photoadaptation of high Arctic ice algae. *Nature* **315**(6016): 219–222.

Cox, GF, Weeks, WF. 1983. Equations for determining the gas and brine volumes in sea-ice samples. *J Glaciol* **29**(102): 306–316. DOI: https://doi.org/10.3189/S0022143000008364.

Deming, JW, Collins, RE. 2017. Sea ice as a habitat for bacteria, archaea and viruses. *Sea Ice* **3**: 326–351.

Desbois, AP, Mearns-Spragg, A, Smith, VJ. 2009. A fatty acid from the diatom *Phaeodactylum tricornutum* is antibacterial against diverse bacteria including multi-resistant *Staphylococcus aureus* (MRSA). *Mar Biotechnol* **11**(1): 45–52. DOI: https://doi.org/10.1007/s10126-008-9118-5.

Desbois, AP, Smith, VJ. 2010. Antibacterial free fatty acids: Activities, mechanisms of action and biotechnological potential. *Appl Microbiol Biotechnol* **85**(6): 1629–1642. DOI: https://doi.org/10.1007/s00253-009-2355-3.

Dupont, F. 2012. Impact of sea-ice biology on overall primary production in a biophysical model of the pan-Arctic Ocean. *J Geophys Res: Oceans* **117**(C8). DOI: https://doi.org/10.1029/2011JC006983.

Eberlein, C, Baumgarten, T, Starke, S, Heipieper, HJ. 2018. Immediate response mechanisms of Gram-negative solvent-tolerant bacteria to cope with environmental stress: *Cis-trans* isomerization of unsaturated fatty acids and outer membrane vesicle secretion. *Appl Microbiol Biotechnol* **102**(6): 2583–2593. DOI: https://doi.org/10.1007/s00253-018-8832-9.

Ewert, M, Deming, J. 2013. Sea ice microorganisms: Environmental constraints and extracellular responses. *Biology* **2**(2): 603–628. DOI: https://doi.org/10.3390/biology2020603.

Ewert, M, Deming, JW. 2014. Bacterial responses to fluctuations and extremes in temperature and brine salinity at the surface of Arctic winter sea ice. *FEMS*

Microbiol Lett **89**(2): 476–489. DOI: https://doi.org/10.1111/1574-6941.12363.

Fahl, K, Kattner, G. 1993. Lipid content and fatty acid composition of algal communities in sea-ice and water from the Weddell Sea (Antarctica). *Polar Biol* **13**(6): 405–409. DOI: https://doi.org/10.1007/BF01681982.

Falk-Petersen, S, Sargent, JR, Henderson, J, Hegseth, EN, Hop, H, Okolodkov, YB. 1998. Lipids and fatty acids in ice algae and phytoplankton from the Marginal Ice Zone in the Barents Sea. *Polar Biol* **20**(1): 41–47. DOI: https://doi.org/10.1007/s003000050274.

Feldlaufer, M, Knox, D, Lusby, W, Shimanuki, H. 1993. Antimicrobial activity of fatty acids against Bacillus larvae, the causative agent of American foulbrood disease. *Apidologie* **24**(2): 95–99. DOI: https://doi.org/10.1051/apido:19930202.

Fernandes, SO, Javanaud, C, Michotey, VD, Guasco, S, Anschutz, P, Bonin, P. 2016. Coupling of bacterial nitrification with denitrification and anammox supports N removal in intertidal sediments (Arcachon Bay, France). *Estuarine, Coastal Shelf Sci* **179**: 39–50. DOI: https://doi.org/10.1016/j.ecss.2015.10.009.

Fernández-Méndez, M, Katlein, C, Rabe, B, Nicolaus, M, Peeken, I, Bakker, K, Flores, H, Boetius, A. 2015. Photosynthetic production in the central Arctic Ocean during the record sea-ice minimum in 2012. *Biogeosciences* **12**(11): 3525–3549. DOI: https://doi.org/10.5194/bg-12-3525-2015.

Firth, E, Carpenter, S, Sørensen, H, Collins, R, Deming, J. 2016. Bacterial use of choline to tolerate salinity shifts in sea-ice brines. *Elem Sci Anth* **4**. DOI: http://doi.org/10.12952/journal.elementa.000120.

Fischer, J, Schauer, F, Heipieper, HJ. 2010. The trans/cis ratio of unsaturated fatty acids is not applicable as biomarker for environmental stress in case of long-term contaminated habitats. *Appl Microbiol Biotechnol* **87**(1): 365–371. DOI: https://doi.org/10.1007/s00253-010-2544-0.

Garrison, DL, Buck, KR. 1987. Algal assemblages in Antarctic pack ice and in ice-edge plankton. *J Phycol* **23**: 564–573. DOI: https://doi.org/10.1111/j.1529-8817.1987.tb04206.x.

Ghiglione, J, Mevel, G, Pujo-Pay, M, Mousseau, L, Lebaron, P, Goutx, M. 2007. Diel and seasonal variations in abundance, activity, and community structure of particle-attached and free-living bacteria in NW Mediterranean Sea. *Microb Ecol* **54**(2): 217–231. DOI: https://doi.org/10.1007/s00248-006-9189-7.

Gosselin, M, Legendre, L, Therriault, JC, Demers, S, Rochet, M. 1986. Physical control of the horizontal patchiness of sea ice microalgae. *Mar Ecol Prog Ser* **29**(3): 289–298.

Gosselin, M, Levasseur, M, Wheeler, PA, Horner, RA, Booth, BC. 1997. New measurements of phytoplankton and ice algal production in the Arctic Ocean. *Deep Sea Research Part II* **44**(8): 1623–1644. DOI: https://doi.org/10.1016/S0967-0645(97)00054-4.

Graeve, M, Kattner, G, Hagen, W. 1994. Diet-induced changes in the fatty acid composition of Arctic herbivorous copepods: Experimental evidence of trophic markers. *J Exp Mar Biol Ecol* **182**(1): 97–110. DOI: https://doi.org/10.1016/0022-0981(94)90213-5.

Greenway, D, Dyke, K. 1979. Mechanism of the inhibitory action of linoleic acid on the growth of *Staphylococcus aureus*. *Microbiology* **115**(1): 233–245. DOI: https://doi.org/10.1099/00221287-115-1-233.

Grenacher, S, Guerin, PM. 1994. Inadvertent introduction of squalene, cholesterol, and other skin products into a sample. *J Chem Ecol* **20**(11): 3017–3025. DOI: https://doi.org/10.1007/BF02098406.

Guckert, J, Hood, M, White, D. 1986. Phospholipid ester-linked fatty acid profile changes during nutrient deprivation of *Vibrio cholerae*: Increases in the *trans/cis* ratio and proportions of cyclopropyl fatty acids. *Appl Environ Microbiol* **52**(4): 794–801.

Guerrero, A, Casals, I, Busquets, M, Leon, Y, Manresa, A. 1997. Oxydation of oleic acid to (*E*)-10-hydroperoxy-8-octadecenoic and (*E*)-10-hydroxy-8-octadecenoic acids by *Pseudomonas sp. 42A2*. *Biochim Biophys Acta* **1347**(1): 75–81. DOI: https://doi.org/10.1016/S0005-2760(97)00056-8.

Hansen, B, Bech, G. 1996. Bacteria associated with a marine planktonic copepod in culture. I. Bacterial genera in seawater, body surface, intestines and fecal pellets and succession during fecal pellet degradation. *J Plankton Res* **18**(2): 257–273. DOI: https://doi.org/10.1093/plankt/18.2.257.

Hare, A, Wang, F, Barber, D, Geilfus, N-X, Galley, R, Rysgaard, S. 2013. pH evolution in sea ice grown at an outdoor experimental facility. *Mar Chem* **154**: 46–54. DOI: https://doi.org/10.1016/j.marchem.2013.04.007.

Harvey, HR, Eglinton, G, O'Hara, SC, Corner, ED. 1987. Biotransformation and assimilation of dietary lipids by Calanus feeding on a dinoflagellate. *Geochim Cosmochim Acta* **51**(11): 3031–3040. DOI: https://doi.org/10.1016/0016-7037(87)90376-0.

Heipieper, HJ, Meinhardt, F, Segura, A. 2003. The cis–trans isomerase of unsaturated fatty acids in *Pseudomonas* and *Vibrio*: Biochemistry, molecular biology and physiological function of a unique stress adaptive mechanism. *FEMS Microbiol Lett* **229**(1): 1–7. DOI: https://doi.org/10.1016/S0378-1097(03)00792-4.

Heipieper, HJ, Neumann, G, Cornelissen, S, Meinhardt, F. 2007. Solvent-tolerant bacteria for biotransformations in two-phase fermentation systems. *Appl Microbiol Biotechnol* **74**(5): 961–973. DOI: https://doi.org/10.1007/s00253-006-0833-4.

Horner, R, Schrader, G. 1982. Relative contributions of ice algae, phytoplankton, and benthic microalgae to primary production in nearshore regions of the Beaufort Sea. *Arctic* **35**(4): 485–503.

Howard-Jones, M, Ballard, V, Allen, A, Frischer, M, Verity, P. 2002. Distribution of bacterial biomass and activity in the marginal ice zone of the central Barents Sea during summer. *J Mar Syst* **38**(1–2): 77–91. DOI: https://doi.org/10.1016/S0924-7963(02)00170-7.

Hu, Q, Sommerfeld, M, Jarvis, E, Ghirardi, M, Posewitz, M, Seibert, M, Darzins, A. 2008. Microalgal triacylglycerols as feedstocks for biofuel production: Perspectives and advances. *Plant J* **54**(4): 621–639. DOI: https://doi.org/10.1111/j.1365-313X.2008.03492.x.

Jacobsen, TR, Azam, F. 1984. Role of bacteria in copepod fecal pellet decomposition: Colonization, growth rates and mineralization. *Bull Mar Sci* **35**(3): 495–502.

Johnsen, G, Sakshaug, E. 1993. Bio-optical characteristics and photoadaptive responses in the toxic and bloom-forming dinoflagellates *Gyrodinium aureolum*, *Gymnodinium galatheanum*, and two strains of *Prorocentrum minimum*. *J Phycol* **29**(5): 627–642. DOI: https://doi.org/10.1111/j.0022-3646.1993.00627.x.

Jüttner, F. 2001. Liberation of 5, 8, 11, 14, 17-eicosapentaenoic acid and other polyunsaturated fatty acids from lipids as a grazer defense reaction in epilithic diatom biofilms. *J Phycol* **37**(5): 744–755. DOI: https://doi.org/10.1046/j.1529-8817.2001.00130.x.

Kaczmarska, I, Ehrman, JM, Bates, SS, Green, DH, Léger, C, Harris, J. 2005. Diversity and distribution of epibiotic bacteria on *Pseudo-nitzschia multiseries* (Bacillariophyceae) in culture, and comparison with those on diatoms in native seawater. *Harmful Algae* **4**: 725–741. DOI: https://doi.org/10.1016/j.hal.2004.10.001.

Katlein, C, Arndt, S, Nicolaus, M, Perovich, DK, Jakuba, MV, Suman, S, Elliott, S, Whitcomb, LL, McFarland, CJ, Gerdes, R, Boetius, A, German, CR. 2015. Influence of ice thickness and surface properties on light transmission through Arctic sea ice. *J Geophys Res: Oceans* **120**(9): 5932–5944.

Khotimchenko, SV, Yakovleva, IM. 2005. Lipid composition of the red alga *Tichocarpus crinitus* exposed to different levels of photon irradiance. *Phytochemistry* **66**(1): 73–79. DOI: https://doi.org/10.1016/j.phytochem.2004.10.024.

Kirchman, DL, Malmstrom, RR, Cottrell, MT. 2005. Control of bacterial growth by temperature and organic matter in the Western Arctic. *Deep Sea Res Part II* **52**(24–26): 3386–3395. DOI: https://doi.org/10.1016/j.dsr2.2005.09.005.

Kjelleberg, S, Hermansson, M, Marden, P, Jones, G. 1987. The transient phase between growth and nongrowth of heterotrophic bacteria, with emphasis on the marine environment. *Annu Rev Microbiol* **41**(1): 25–49.

Krembs, C, Eicken, H, Deming, JW. 2011. Exopolymer alteration of physical properties of sea ice and implications for ice habitability and biogeochemistry in a warmer Arctic. *Proc Natl Acad Sci* **108**(9): 3653–3658. DOI: https://doi.org/10.1073/pnas.1100701108.

Lavoie, D, Denman, K, Michel, C. 2005. Modeling ice algal growth and decline in a seasonally ice-covered region of the Arctic (Resolute Passage, Canadian Archipelago). *J Geophys Res* **110**(C11). DOI: https://doi.org/10.1029/2005JC002922.

Lee, SH, Whitledge, TE. 2005. Primary and new production in the deep Canada Basin during summer 2002. *Polar Biol* **28**(3): 190–197. DOI: https://doi.org/10.1007/s00300-004-0676-3.

Leu, E, Wiktor, J, Søreide, JE, Berge, J, Falk-Petersen, S. 2010. Increased irradiance reduces food quality of sea ice algae. *Mar Ecol Prog Ser* **411**: 49–60. DOI: https://doi.org/10.3354/meps08647.

Lizotte, M, Levasseur, M, Law, CS, Walker, CF, Safi, KA, Marriner, A, Kiene, RP. 2017. Dimethylsulfoniopropionate (DMSP) and dimethyl sulfide (DMS) cycling across contrasting biological hotspots of the New Zealand subtropical front. *Ocean Sci* **13**(6). DOI: https://doi.org/10.5194/os-2017-32.

Loffeld, B, Keweloh, H. 1996. Cis/trans isomerization of unsaturated fatty acids as possible control mechanism of membrane fluidity in *Pseudomonas putida* P8. *Lipids* **31**(8): 811–815. DOI: https://doi.org/10.1007/BF02522976.

Loose, B, Miller, LA, Elliott, S, Papakyriakou, T. 2011. Sea ice biogeochemistry and material transport across the frozen interface. *Oceanography* **24**(3): 202–218.

Macnaughton, MO, Thormar, J, Berge, J. 2007. Sympagic amphipods in the Arctic pack ice: Redescriptions of *Eusirus holmii Hansen*, 1887 and *Pleusymtes karstens*i (Barnard, 1959). *Polar Biol* **30**(8): 1013–1025. DOI: https://doi.org/10.1007/s00300-007-0260-8.

Maranger, R, Bird, DF, Juniper, SK. 1994. Viral and bacterial dynamics in Arctic sea ice during the spring algal bloom near Resolute, NWT, Canada. *Mar Ecol Prog Ser* **111**: 121–127.

Marie, D, Partensky, F, Jacquet, S, Vaulot, D. 1997. Enumeration and cell cycle analysis of natural populations of marine picoplankton by flow cytometry using the nucleic acid stain SYBR Green I. *Appl Environ Microbiol* **63**(1): 186–193.

Marie, D, Rigaut-Jalabert, F, Vaulot, D. 2014. An improved protocol for flow cytometry analysis of phytoplankton cultures and natural samples. *Cytometry Part A* **85**(11): 962–968. DOI: https://doi.org/10.1002/cyto.a.22517.

Martínez, E, Hamberg, M, Busquets, M, Díaz, P, Manresa, A, Oliw, EH. 2010. Biochemical characterization of the oxygenation of unsaturated fatty acids by the dioxygenase and hydroperoxide isomerase of *Pseudomonas aeruginosa 42A2*. *J Biol Chem* **285**(13): 9339–9345. DOI: https://doi.org/10.1074/jbc.M109.078147.

Massicotte, P, Amiraux, R, Amyot, M-P, Archambault, P, Ardyna, M, Arnaud, L, Artigue, L, Aubry, C, Ayotte, P, Bécu, G, Bélanger, S, Benner, R, Bittig, HC, Bricaud, A, Brossier, É, Bruyant, F,

Chauvaud, L, Christiansen-Stowe, D, Claustre, H, Cornet-Barthaux, V, Coupel, P, Cox, C, Delaforge, A, Dezutter, T, Dimier, C, Domine, F, Dufour, F, Dufresne, C, Dumont, D, Ehn, J, Else, B, Ferland, J, Forget, M-H, Fortier, L, Galí, M, Galindo, V, Gallinari, M, Garcia, N, Ribeiro, CG, Gourdal, M, Gourvil, P, Goyens, C, Grondin, P-L, Guillot, P, Guilmette, C, Houssais, M-N, Joux, F, Lacour, L, Lacour, T, Lafond, A, Lagunas, J, Lalande, C, Laliberté, J, Lambert-Girard, S, Larivière, J, Lavaud, J, LeBaron, A, Leblanc, K, Le Gall, F, Legras, J, Lemire, M, Levasseur, M, Leymarie, E, Leynaert, A, dos Santos, AL, Lourenço, A, Mah, D, Marec, C, Marie, D, Martin, N, Marty, C, Marty, S, Massé, G, Matsuoka, A, Matthes, L, Moriceau, B, Muller, P-E, Mundy, C-J, Neukermans, G, Oziel, L, Panagiotopoulos, C, Pangrazi, J-J, Picard, G, Picheral, M, du Sel, FP, Pogorzelec, N, Probert, I, Quéguiner, B, Raimbault, P, Ras, J, Rehm, E, Reimer, E, Rontani, J-F, Rysgaard, S, Saint-Béat, B, Sampei, M, Sansoulet, J, Schmechtig, C, Schmidt, S, Sempéré, R, Sévigny, C, Shen, Y, Tragin, M, Tremblay, J-É, Vaulot, D, Verin, G, Vivier, F, Vladoiu, A, Whitehead, J, Babin, M. 2020. Green Edge ice camp campaigns: Understanding the processes controlling the under-ice Arctic phytoplankton spring bloom. *Earth Syst Sci Data* **12**: 151–176. DOI: https://doi.org/10.5194/essd-2019-160.

Massicotte, P, Bécu, G, Lambert-Girard, S, Leymarie, E, Babin, M. 2018. Estimating underwater light regime under spatially heterogeneous sea ice in the Arctic. *Appl Sci* **8**(12): 2693. DOI: https://doi.org/10.3390/app8122693.

Meiners, K, Krembs, C, Gradinger, R. 2008. Exopolymer particles: Microbial hotspots of enhanced bacterial activity in Arctic fast ice (Chukchi Sea). *Aquat Microb Ecol* **52**(2): 195–207. DOI: https://doi.org/10.3354/ame01214.

Michotey, V, Guasco, S, Boeuf, D, Morezzi, N, Durieux, B, Charpy, L, Bonin, P. 2012. Spatio-temporal diversity of free-living and particle-attached prokaryotes in the tropical lagoon of Ahe atoll (Tuamotu Archipelago) and its surrounding oceanic waters. *Marine Pollution Bulletin* **65**(10–12): 525–537. DOI:10.1016/j.marpolbul.2012.01.009.

Mikkelsen, DM, Rysgaard, S, Glud, RN. 2008. Microalgal composition and primary production in Arctic sea ice: A seasonal study from Kobbeijord (Kangerluarsunnguaq), West Greenland. *Mar Ecol Prog Ser* **368**: 65–74. DOI: https://doi.org/10.3354/meps07627.

Miller, LA, Fripiat, F, Else, BG, Bowman, JS, Brown, KA, Collins, RE, Ewert, M, Fransson, A, Gosselin, M, Lannuzel, D, Meiners, KM, Michel, C, Nishioka, J, Nomura, D, Papadimitriou, S, Russell, LM, Sørensen, LL, Thomas, DN, Tison, J-L, van Leeuwe, MA, Vancoppenolle, M, Wolff, EW, Zhou, J. 2015. Methods for biogeochemical studies of sea ice: The state of the art, caveats, and recommendations. *Elem Sci Anth* **3**. DOI: https://doi.org/10.12952/journal.elementa.000038.

Mock, T, Junge, K. 2007. Psychrophilic diatoms, in *Algae and cyanobacteria in extreme environments*. Dordrecht: Springer: 343–364. DOI: https://doi.org/10.1007/978-1-4020-6112-7_18.

Monfort, P, Demers, S, Levasseur, M. 2000. Bacterial dynamics in first year sea ice and underlying seawater of Saroma-ko Lagoon (Sea of Okhotsk, Japan) and Resolute Passage (High Canadian Arctic): Inhibitory effects of ice algae on bacterial dynamics. *Can J Microbiol* **46**(7): 623–632. DOI: https://doi.org/10.1139/w00-024.

Nocker, A, Cheung, C-Y, Camper, AK. 2006. Comparison of propidium monoazide with ethidium monoazide for differentiation of live vs. dead bacteria by selective removal of DNA from dead cells. *J Microbiol Methods* **67**(2): 310–320. DOI: https://doi.org/10.1016/j.mimet.2006.04.015.

Nocker, A, Mazza, A, Masson, L, Camper, AK, Brousseau, R. 2009. Selective detection of live bacteria combining propidium monoazide sample treatment with microarray technology. *J Microbiol Methods* **76**(3): 253–261. DOI: https://doi.org/10.1016/j.mimet.2008.11.004.

Oziel, L, Massicotte, P, Randelhoff, A, Ferland, J, Vladoiu, A, Lacour, L, Galindo, V, Lambert-Girard, S, Dumont, D, Cuypers, Y, Bouruet-Aubertot, P, Mundy, C-J, Ehn, J, Bécu, G, Marec, C, Forget, M-H, Garcia, N, Coupel, P, Raimbault, P, Houssais, M-N, Babin, M. 2019. Environmental factors influencing the seasonal dynamics of under-ice spring blooms in Baffin Bay. *Elem Sci Anth* **7**(1): 34. DOI: http://doi.org/10.1525/elementa.372.

Pabi, S, van Dijken, GL, Arrigo, KR. 2008. Primary production in the Arctic Ocean, 1998–2006. *J Geophys Res: Oceans* **113**(C8). DOI: https://doi.org/10.1029/2007JC004578.

Parrish, CC. 2013. Lipids in marine ecosystems. *ISRN Oceanography* **2013**. DOI: https://doi.org/10.5402/2013/604045.

Parsons, T, Maita, Y, Lalli, C. 1984. *A manual of chemical and biological methods for seawater analysis*. Toronto, Canada: Pergamon Press.

Pedersen, L, Jensen, HM, Burmeister, A, Hansen, BW. 1999. The significance of food web structure for the condition and tracer lipid content of juvenile snail fish (Pisces: *Liparis spp.*) along 65-72°N off West Greenland. *J Plankton Res* **21**: 1593–1611. DOI: https://doi.org/10.1093/plankt/21.9.1593.

Perovich, DK. 1996. *The optical properties of sea ice* [Monograph]. Hanover, NH: Cold Regions Research and Engineering Lab. 25 pp.

Platt, T, Gallegos, CL. 1980. Modelling primary production, in Falkowski, PG ed., Primary productivity in the sea. *Environmental Science Research*, vol 19. Boston, MA: Springer: 339–362. DOI: https://doi.org/10.1007/978-1-4684-3890-1_19.

Pomeroy, LR, Deibel, D. 1986. Temperature regulation of bacterial activity during the spring bloom in

Newfoundland coastal waters. *Science* **233**(4761): 359–361. DOI: https://doi.org/10.1126/science.233.4761.359.

Pomeroy, LR, Wiebe, WJ. 2001. Temperature and substrates as interactive limiting factors for marine heterotrophic bacteria. *Aquat Microb Ecol* **23**(2): 187–204. DOI: https://doi.org/10.3354/ame023187.

Popova, E, Yool, A, Coward, A, Aksenov, Y, Alderson, S, de Cuevas, BA, Anderson, TR. 2010. Control of primary production in the Arctic by nutrients and light: Insights from a high resolution ocean general circulation model. *Biogeosciences* **7**(11): 3569–3591. DOI: https://doi.org/10.5194/bgd-7-5557-2010.

Ralph, PJ, Ryan, KG, Martin, A, Fenton, G. 2007. Melting out of sea ice causes greater photosynthetic stress in algae than freezing in 1. *J Phycol* **43**(5): 948–956.

Rampen, SW, Abbas, BA, Schouten, S, Damsté, JSS. 2010. A comprehensive study of sterols in marine diatoms (Bacillariophyta): Implications for their use as tracers for diatom productivity. *Limnol Oceanogr* **55**(1): 91–105. DOI: https://doi.org/10.4319/lo.2010.55.1.0091.

Reuss, N, Poulsen, L. 2002. Evaluation of fatty acids as biomarkers for a natural plankton community. A field study of a spring bloom and a post-bloom period off West Greenland. *Mar Biol* **141**(3): 423–434. DOI: https://doi.org/10.1007/s00227-002-0841-6.

Riebesell, U, Schloss, I, Smetacek, V. 1991. Aggregation of algae released from melting sea ice: Implications for seeding and sedimentation. *Polar Biol* **11**(4): 239–248. DOI: https://doi.org/10.1007/BF00238457.

Riedel, A, Michel, C, Gosselin, M. 2006. Seasonal study of sea-ice exopolymeric substances on the Mackenzie shelf: Implications for transport of sea-ice bacteria and algae. *Aquat Microb Ecol* **45**(2): 195–206. DOI: https://doi.org/doi:10.3354/ame045195.

Rivkin, RB, Anderson, M, Lajzerowicz, C. 1996. Microbial processes in cold oceans. I. Relationship between temperature and bacterial growth rate. *Aquat Microb Ecol* **10**(3): 243–254. DOI: https://doi.org/10.3354/ame010243.

Sakshaug, E. 2004. Primary and secondary production in the Arctic Seas, in Stein, R, Macdonald, RW eds., *The organic carbon cycle in the Arctic ocean*. London, UK: Springer: 57–81.

Sampei, M, Fortier, L, Raimbault, P, Matsuno, K, Abe, Y, Babin, M, Hirawake, T. An estimation of quantitative impacts of copepod grazing on under-ice phytoplankton spring bloom in western Baffin Bay, Canadian Arctic. *Elem Sci Anth* (under review).

Shin, SY, Bajpai, VK, Kim, HR, Kang, SC. 2007. Antibacterial activity of bioconverted eicosapentaenoic (EPA) and docosahexaenoic acid (DHA) against foodborne pathogenic bacteria. *Int J Food Microbiol* **113**(2): 233–236. DOI: https://doi.org/10.1016/j.ijfoodmicro.2006.05.020.

Shoja Chaghervand, S. 2019. Characterization of the enzymes involved in the diolsynthase pathway in *Pseudomonas aeruginosa* [PhD thesis]. Barcelona, Universitat de Barcelona. Available at http://diposit.ub.edu/dspace/bitstream/2445/139344/1/SSC_PhD_THESIS.pdf. Accessed 7 December, 2019.

Sicre, M-A, Paillasseur, J-L, Marty, J-C, Saliot, A. 1988. Characterization of seawater samples using chemometric methods applied to biomarker fatty acids. *Org Geochem* **12**(3): 281–288. DOI: https://doi.org/10.1016/0146-6380(88)90265-3.

Sinensky, M. 1974. Homeoviscous adaptation—A homeostatic process that regulates the viscosity of membrane lipids in *Escherichia coli*. *Proc Natl Acad Sci* **71**(2): 522–525. DOI: https://doi.org/10.1073/pnas.71.2.522.

Small, L, Fowler, S, Ünlü, M. 1979. Sinking rates of natural copepod fecal pellets. *Mar Biol* **51**(3): 233–241. DOI: https://doi.org/10.1007/BF00386803.

Smith, RE, Clement, P, Cota, GF. 1989. Population dynamics of bacteria in Arctic sea ice. *Microb Ecol* **17**(1): 63–76. DOI: https://doi.org/10.1007/BF02025594.

Smith, REH, Cavaletto, JF, Eadie, BJ, Gardner, WS. 1993. Growth and lipid composition of high Arctic ice algae during the spring bloom at Resolute, Northwest Territories, Canada. *Mar Ecol Prog Ser* **97**(1): 19–29.

Smith, SD, Muench, RD, Pease, CH. 1990. Polynyas and leads: An overview of physical processes and environment. *J Geophys Res: Oceans* **95**(C6): 9461–9479.

Søreide, JE, Leu, E, Berge, J, Graeve, M, Falk-Petersen, S. 2010. Timing of blooms, algal food quality and *Calanus glacialis* reproduction and growth in a changing Arctic. *Glob Change Biol* **16**(11): 3154–3163. DOI: https://doi.org/10.1111/j.1365-2486.2010.02175.x.

Takai, K, Horikoshi, K. 2000. Rapid detection and quantification of members of the archaeal community by quantitative PCR using fluorogenic probes. *Appl Environ Microbiol* **66**(11): 5066–5072. DOI: https://doi.org/10.1128/AEM.66.11.5066-5072.2000.

Thomas, DN, Papadimitriou, S. 2003. Biogeochemistry of sea ice, in Thomas, DN, Dieckmann, GS eds., *Sea Ice: An introduction to its physics, chemistry, biology and geology*. Oxford: Blackwell: 267–332.

Tison, J-L, Brabant, F, Dumont, I, Stefels, J. 2010. High resolution DMS and DMSP time series profiles in decaying summer first-year sea ice at ISPOL (Western Weddell Sea, Antarctica). *J Geophys Res* **115**. DOI: https://doi.org/10.1029/2010JG001427.

Tremblay, J-É, Robert, D, Varela, DE, Lovejoy, C, Darnis, G, John Nelson, R, Sastri, AR. 2012. Current state and trends in Canadian Arctic marine ecosystems: I. Primary production. *Clim Change* **115**(1): 161–178. DOI: https://doi.org/10.1007/s10584-012-0496-3.

Volkman, J. 2003. Sterols in microorganisms. *Appl Microbiol Biotechnol* **60**(5): 495–506.

Volkman, JK. 1986. A review of sterol markers for marine and terrigenous organic matter. *Org Geochem* **9**(2):

83–99. DOI: https://doi.org/10.1016/0146-6380(86)90089-6.

Wadhams, P, Martin, S. 2001. Ice in the ocean. *Arctic* **54**(2): 192.

Wassmann, P, Duarte, CM, Agust, ÍS, Sejr, MK. 2011. Footprints of climate change in the Arctic marine ecosystem. *Glob Change Biol* **17**(2): 1235–1249. DOI: https://doi.org/10.1111/j.1365-2486.2010.02311.x.

Wichard, T, Gerecht, A, Boersma, M, Poulet, SA, Wiltshire, K, Pohnert, G. 2007. Lipid and fatty acid composition of diatoms revisited: Rapid wound-activated change of food quality parameters influences herbivorous copepod reproductive success. *ChemBioChem* **8**(10): 1146–1153. DOI: https://doi.org/10.1002/cbic.200700053.

Yager, PL, Deming, JW. 1999. Pelagic microbial activity in an arctic polynya: Testing for temperature and substrate interactions using a kinetic approach. *Limnol Oceanogr* **44**(8): 1882–1893. DOI: https://doi.org/10.4319/lo.1999.44.8.1882.

How to cite this article: Amiraux, R, Burot, C, Bonin, P, Massé, G, Guasco, S, Babin, M, Vaultier, F, Rontani, J-F. 2020. Stress factors resulting from the Arctic vernal sea-ice melt: Impact on the viability of bacterial communities associated with sympagic algae. *Elem Sci Anth*. 8: xx. DOI: https://doi.org/10.1525/elementa.076.

Domain Editor-in-Chief: Jody W. Deming, University of Washington, WA, USA

Associate Editor: Jeff S. Bowman, Scripps Institution of Oceanography, CA, USA

Knowledge Domain: Ocean Science

Part of an Elementa Special Feature: Green Edge

Published: 00, 0000 **Accepted:** October 07, 2020 **Submitted:** November 21, 2020

ELEMENTA Science of the Anthropocene

Elem Sci Anth is a peer-reviewed open access journal published by University of California Press.

OPEN ACCESS